R-10-41

Groundwater flow modelling of an abandoned partially open repository

Niclas Bockgård, Golder Associates AB

December 2010

Svensk Kärnbränslehantering AB
Swedish Nuclear Fuel
and Waste Management Co

Box 250, SE-101 24 Stockholm
Phone +46 8 459 84 00

ISSN 1402-3091
SKB R-10-41

Groundwater flow modelling of an abandoned partially open repository

Niclas Bockgård, Golder Associates AB

December 2010

Keywords: SKBdoc 1247472, Forsmark, Groundwater, Flow model, Repository, Abandoned, Open tunnels, Flow paths, Travel time, DarcyTools, Ice sheet.

Abstract

As a part of the license application, according to the nuclear activities act, for a final repository for spent nuclear fuel at Forsmark, the Swedish Nuclear Fuel and Waste Management Company (SKB) has undertaken a series of groundwater flow modelling studies. These represent time periods with different hydraulic conditions and the simulations carried out contribute to the overall evaluation of the repository design and long-term radiological safety.

The modelling study presented here serves as an input for analyses of so-called future human actions that may affect the repository. The objective of the work was to investigate the hydraulic influence of an abandoned partially open repository. The intention was to illustrate a pessimistic scenario of the effect of open tunnels in comparison to the reference closure of the repository. The effects of open tunnels were studied for two situations with different boundary conditions: A "temperate" case with present-day boundary conditions and a generic future "glacial" case with an ice sheet covering the repository. The results were summarized in the form of analyses of flow in and out from open tunnels, the effect on hydraulic head and flow in the surrounding rock volume, and transport performance measures of flow paths from the repository to surface.

Sammanfattning

I Svensk Kärnbränslehanterings (SKB) ansökan enligt kärntekniklagen om ett slutförvar för använt kärnbränsle i Forsmark ingår olika grundvattenmodelleringsstudier. Studierna hanterar perioder med olika hydrauliska förhållanden och beräkningsresultaten från simuleringarna bidrar till bedömningsunderlaget inom design och långsiktig säkerhet.

Modelleringsstudien som presenteras i denna rapport fungerar som ett underlag för analyser av hur framtida mänskliga aktiviteter kan påverka slutförvaret. Syftet med arbetet var att studera de hydrauliska effekterna av ett övergivet slutförvar med delvis kvarlämnade öppna tunnlar. Avsikten var att illustrera de värsta tänkbara hydrauliska effekterna av öppna tunnlar och att sätta dem i relation till referensfallet med ett fullständigt förslutet förvar. Effekterna av öppna tunnlar studerades för två situationer med olika randvillkor: En situation med tempererade förhållanden med randvillkor som motsvarar dagens förhållanden, och en hypotetisk framtida glacial situation med ett istäcke som täcker förvaret. Resultaten sammanställdes i form av analyser av flöden in i och ut ur öppna tunnlar, effekter på hydraulisk potential och grundvattenströmning i den omgivande bergvolymen samt som olika statistiska mått på egenskaperna för flödesbanor från förvaret till markytan.

Contents

1 Introduction

1.1 Background

The Swedish Nuclear Fuel and Waste Management Company (SKB) has conducted site investigations at two different locations, the Forsmark and Laxemar-Simpevarp areas (Figure 1-1), with the objective of siting a final repository for spent nuclear fuel according to the KBS-3 concept. As a part of the application for a final repository for spent nuclear fuel at Forsmark, information from a series of groundwater flow modelling studies is evaluated to serve as a basis for an assessment of the repository design and long-term radiological safety premises. The present report serves as an input for analyses of so called future human actions that may affect the repository /SKB 2010b/.

1.2 Scope and objectives

The main objective of the work reported here was to investigate the hydraulic influence of future human actions in the form of an abandoned partially open repository. However, the intention was not to fully represent a true future groundwater flow situation at Forsmark. The intention was to illustrate a pessimistic scenario of the effect of open tunnels in comparison to the reference closure of the repository. The effects of open tunnels were studied for two situations with different boundary conditions: A "temperate" situation with present-day boundary conditions and a generic future "glacial" situation with an ice sheet covering the repository.

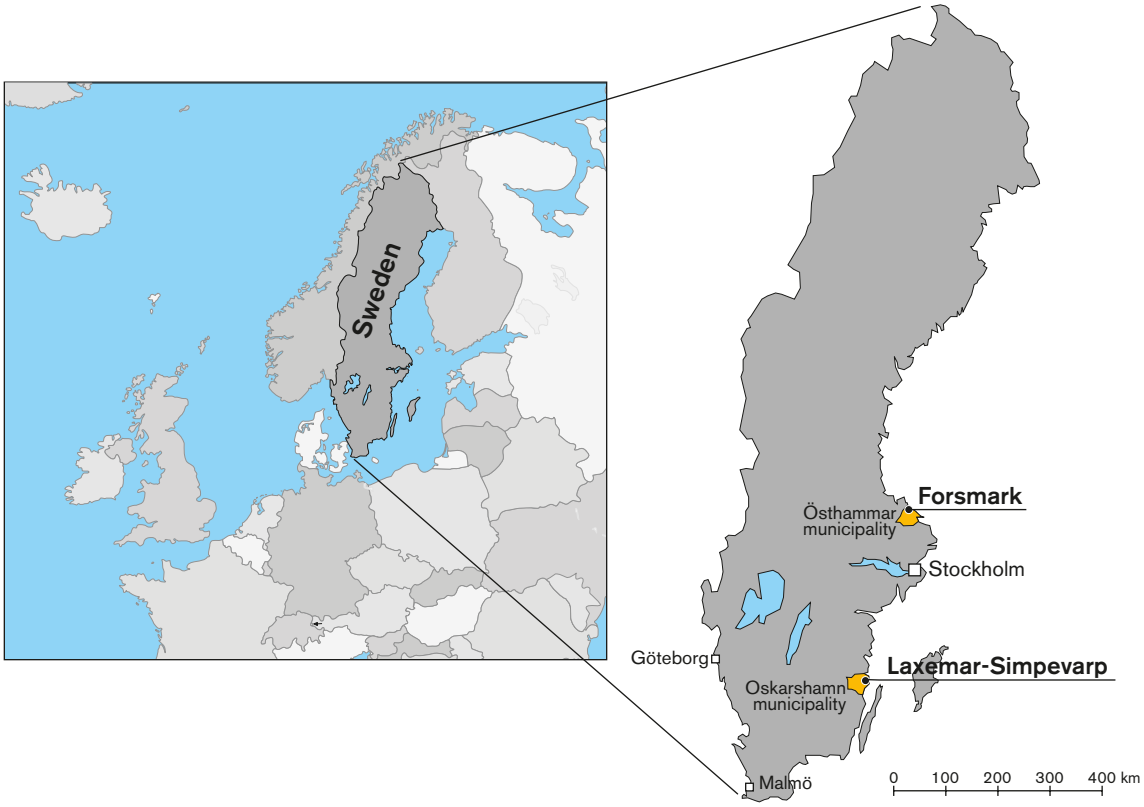

Figure 1-1. *Map of Sweden showing the location of the Forsmark and Laxemar-Simpevarp sites, located in the municipalities of Östhammar and Oskarshamn, respectively. (Figure 1-1 in /SKB 2008/.)*

Specific objectives were to study the flow in and out from open tunnels, the effect on hydraulic head and flow in the surrounding rock volume, and to make flow-path analyses. The following performance measures were studied:

- Hydraulic head changes.
- Darcy flux at repository depth.
- Advective travel times, flow-path lengths, and flow-related transport resistances (F-factor) of particles travelling from the repository to the surface.

All simulations were steady-state simulations. Density-driven flow was not included in the model, nor effects of heat flux from the repository. Ignoring salinity/density variations simplified the modelling approach considerably and supported the use of a steady-state model. The assumption of constant density is in general conservative /Avis et al. 2009/ since an increasing groundwater density with depth tends to decrease vertical hydraulic gradients. The numerical groundwater flow and transport modelling was performed using the version 3.3 of the DarcyTools simulation code (see Chapter 2).

1.3 Setting

The Forsmark area is located in northern Uppland within the municipality of Östhammar, about 120 km north of Stockholm (Figure 1-2). The candidate area for site investigation is located along the shoreline of Öregrundsgrepen. It extends from the Forsmark nuclear power plant and the access road to SFR in the north-west (SFR is an existing repository for short-lived radioactive waste) to Kallrigafjärden in the south-east (Figure 1-2). It is approximately 6 km long and 2 km wide. The north-western part of the candidate area was selected as the target area for the complete site investigation work /SKB 2005b/ (Figure 1-3).

The Forsmark area consists of crystalline bedrock that belongs to the Fennoscandian Shield, one of the ancient continental nuclei on the Earth. The bedrock at Forsmark in the south-western part of this shield formed between 1,890 and 1,850 million years ago during the Svecokarelian orogeny /SKB 2005a/. It has been affected by both ductile and brittle deformation. The ductile deformation has resulted in large-scale, ductile high-strain belts and more discrete high-strain zones. Tectonic lenses, in which the bedrock is less affected by ductile deformation, are enclosed between the ductile high strain belts. The candidate area is located in the north-westernmost part of one of these tectonic lenses. This lens extends from north-west of the nuclear power plant south-eastwards to the area around Öregrund (Figure 1-4). The brittle deformation has given rise to reactivation of the ductile zones in the colder, brittle regime and the formation of new fracture zones with variable size.

The current ground surface in the Forsmark region forms a part of the sub-Cambrian peneplain in south-eastern Sweden. This peneplain represents a relatively flat topographic surface with a gentle dip towards the east that formed more than 540 million years ago. The candidate area at Forsmark is characterised by a small-scale topography at low altitude (Figure 1-5). The most elevated areas to the south-west of the candidate area are located at c. 25 m above current sea level (datum RHB 70). The whole area is located below the highest coastline associated with the last glaciation, and large parts of the candidate area emerged from the Baltic Sea only during the last 2,000 years. Both the flat topography and the still ongoing shore level displacement of c. 6 mm per year strongly influence the current landscape (Figure 1-5). Sea bottoms are continuously transformed into new terrestrial areas or freshwater lakes, and lakes and wetlands are successively covered by peat.

The site description SDM-Site concluding the site investigations at Forsmark is compiled in /SKB 2008/. The bedrock hydrogeological model is presented in more detail in /Follin 2008/.

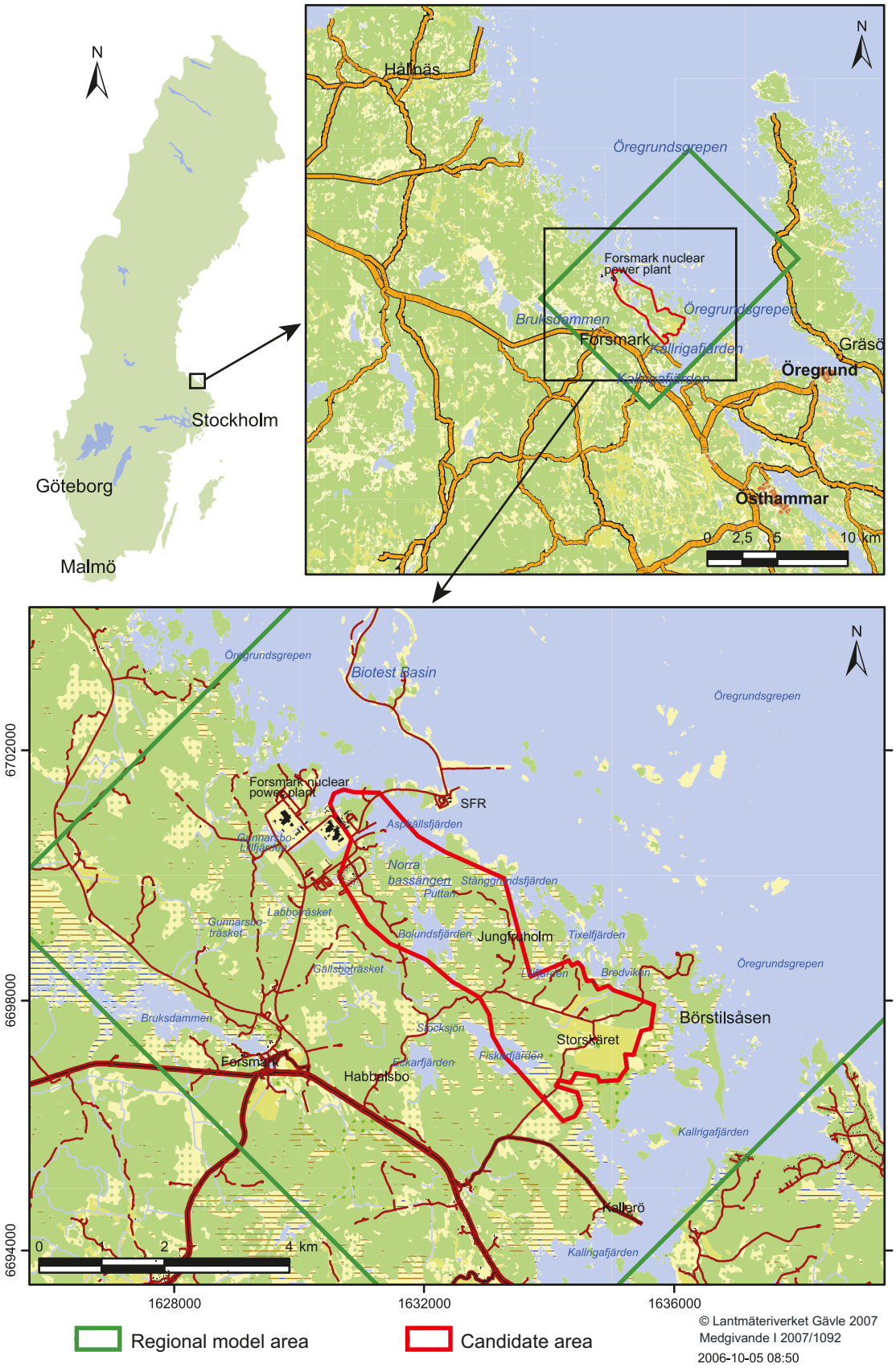

Figure 1-2. *The red polygon shows the size and location of the candidate area for site investigations at Forsmark. The green rectangle indicates the size and location of the regional model area for SDM-Site Forsmark. (Figure 1-3 in /SKB 2008/.)*

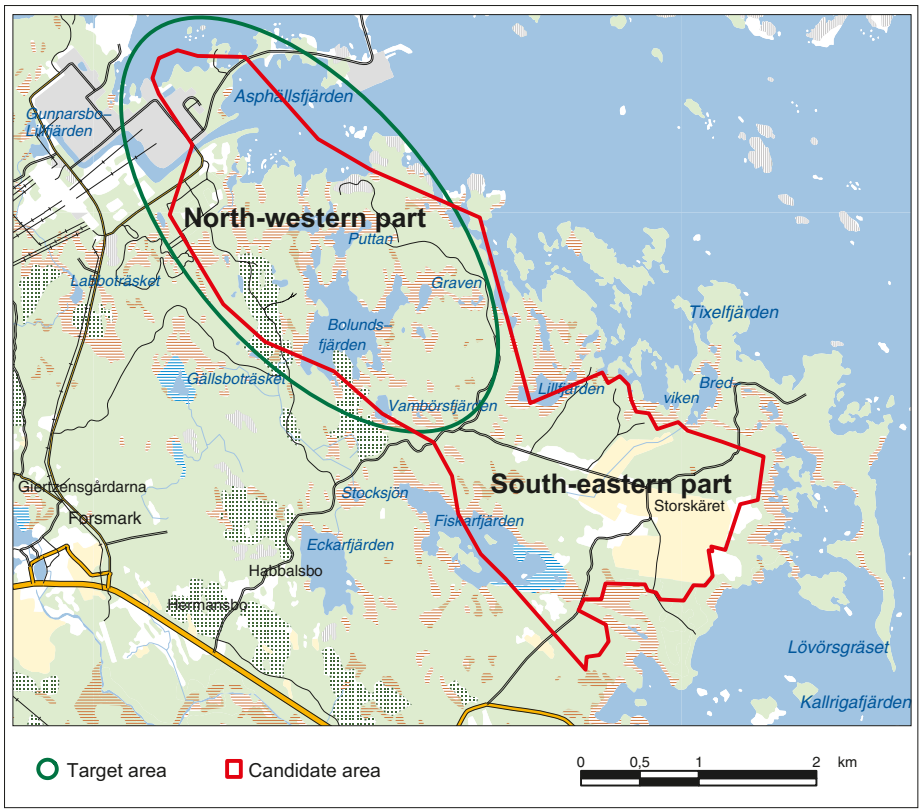

Figure 1-3. *The north-western part of the candidate area was selected as the target area for the complete site investigation work. (Modified after Figure 2-15 in /SKB 2005b/.)*

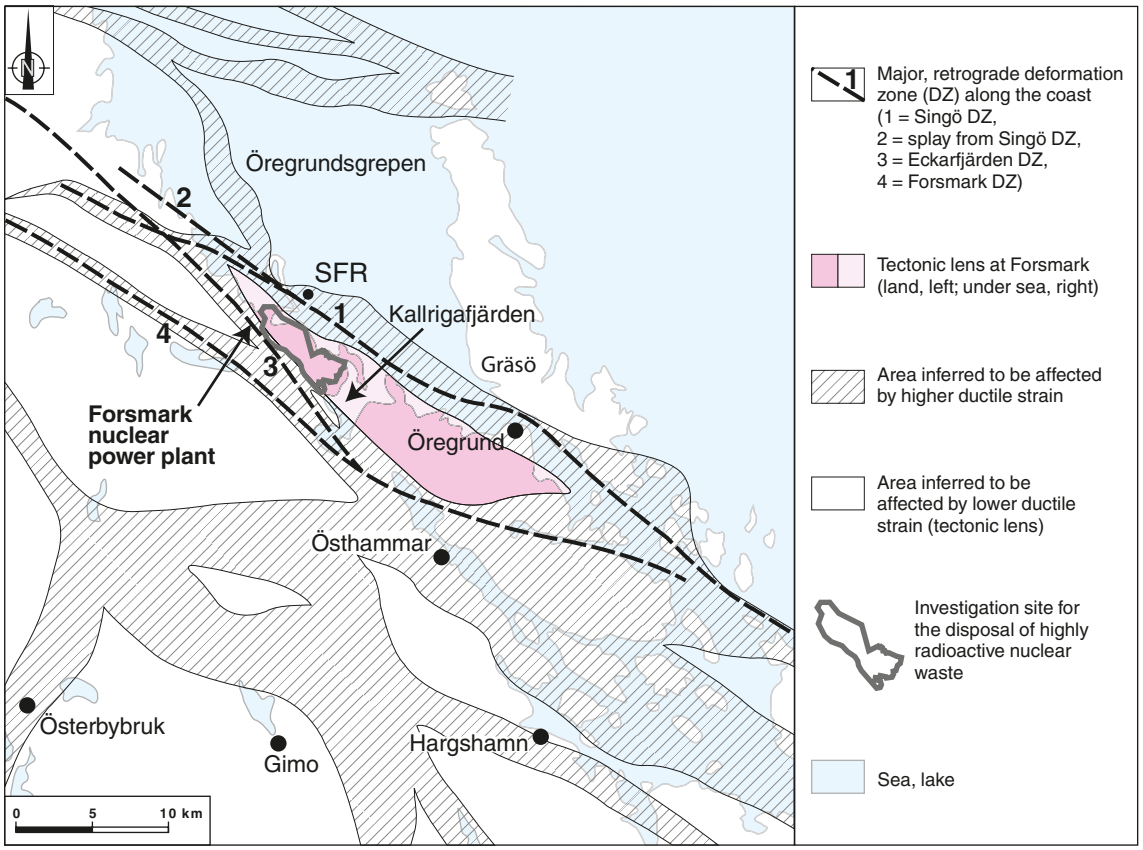

Figure 1-4. *Tectonic lens at Forsmark and areas affected by strong ductile deformation in the area close to Forsmark. (Figure 4-1 in /Stephens et al. 2007/.)*

Figure 1-5. *Photos from Forsmark showing the flat topography and the low-gradient shoreline with recently isolated bays due to land uplift. (Figure 1-7 in /Follin 2008/.)*

1.4 This report

/Selroos and Follin 2010/ present the data and hydraulic properties from the SDM work as well as the methodology to be used by the groundwater flow modelling studies that serve as a basis for an assessment of the design and long-term radiological safety of a final repository at Forsmark in the SR-Site project.

Chapter 2 presents the primary concepts and methodology of the DarcyTools computational model /Svensson et al. 2010/.

Chapter 3 provides a description of the setup of the studied cases (scenarios) and the modelling methodology.

Chapter 4 presents the results of the flow simulations. Chapter 4.1 describes the temperate period, and Chapter 4.2 describes the glacial cases.

Chapter 5 discusses the simulation results and their dependence on the assumptions made and other modelling premises. Finally, Chapter 6 presents the conclusions drawn.

The report contains two appendices, A and B, with the objective to describe and document some key assumptions of the models applied in the work reported here, and for the sake of traceability, consistency and quality assurance.

- Appendix A lists all files with input data and other parameter values, which were imported and used to parameterise the groundwater flow model reported here.
- The set-up of the EPANET 2 pipe network model of the Forsmark repository that was used to calculate the flow through the tunnel system during glacial conditions is documented in Appendix B.

2 Concepts and methodology of DarcyTools

The following section describing the concepts and methodology of DarcyTools is extracted from /Svensson and Follin 2010/.

2.1 Governing equations

Coupled groundwater flow, salt transport, and heat flow in fractured rocks that gives rise to variations in salinity and hence fluid density are in DarcyTools modelled according to the following formulation of the mass conservation equation:

$$\frac{\partial \rho\phi}{\partial t} + \frac{\partial}{\partial x}(\rho u) + \frac{\partial}{\partial y}(\rho v) + \frac{\partial}{\partial z}(\rho w) = Q \tag{2-1}$$

where ρ is fluid density [ML^{-3}], ϕ is the kinematic porosity [–], t is time [T], (u, v, w) are the directional components of the volumetric (Darcy) flux [LT^{-1}] at the location (x, y, z) [L,L,L] in a Cartesian coordinate system, and Q is a source/sink term per unit volume of fluid mass [$ML^{-3}T^{-1}$]. The mass conservation equation is turned into a pressure equation by invoking the assumptions behind Darcy's law:

$$\begin{aligned} \rho u &= -\frac{K_x}{g}\frac{\partial P}{\partial x} \\ \rho v &= -\frac{K_y}{g}\frac{\partial P}{\partial y} \\ \rho w &= -\frac{K_z}{g}\frac{\partial P}{\partial z} - K_z(\rho - \rho_0) \end{aligned} \tag{2-2}$$

where K_x, K_y and K_z are the orthogonal components of the hydraulic conductivity tensor parallel to the Cartesian coordinate system [LT^{-1}], g is the acceleration of gravity [LT^{-2}], ρ_0 is a reference fluid density [ML^{-3}], and P is the dynamic (residual) fluid pressure [$ML^{-1}T^{-2}$] at the location (x, y, z):

$$P = p + \rho_0 g z \tag{2-3}$$

where ρ is the total pressure and ρ_0 g z is the reference hydrostatic pressure, P_0.

The hydraulic conductivity K is related to the permeability k [L^2] through the relation:

$$K = \frac{\rho}{g\mu}k \tag{2-4}$$

where μ is the fluid dynamic viscosity [$ML^{-1}T^{-1}$].

2.2 Methodology

2.2.1 Finite volume method

A detailed description of the concepts and methodology of DarcyTools is found in /Svensson et al. 2010/. DarcyTools uses a staggered computational grid, which means that scalar entities such as pressure, flow porosity and salinity use a cell-centred mesh, whereas directional entities such as hydraulic conductivity, hydrodynamic diffusivity, mass flux, and Darcy flux use a mesh centred at the cell walls. This grid arrangement was first introduced by /Harlow and Welch 1965/ and is described in textbooks, e.g. /Patankar 1980/. Each variable is assumed to be representative for a

certain control volume, which is the volume the equations are formulated for. DarcyTools uses the finite volume method to transform the differential equations into algebraic equations of the type:

$$a_P\Phi_P = a_W\Phi_W + a_E\Phi_E + a_S\Phi_S + a_{\mathrm{N}}\Phi_{\mathrm{N}} + a_{\mathrm{B}}\Phi_{\mathrm{B}} + a_{\mathrm{T}}\Phi_{\mathrm{T}} + S_\phi \quad (2\text{-}5)$$

where Φ denotes the variable in question, a_i are directional coefficients (West, East, South, North, Bottom, and Top) and S_ϕ source/sink terms. The equations are solved by the MIGAL multi-grid equation solver.

2.2.2 Representation of fractures and discrete fracture networks

Principle

The principle used to represent hydraulic properties of discrete fractures as equivalent grid cell hydraulic properties in DarcyTools works as follows: A fracture variable (P_f) contributes to the grid cell variable (P_c) by an amount which is equal to the intersecting volume of the fracture (V_f) times the value of the fracture variable. Contributions from all fractures (N) that intersect the control volume are added and the sum is divided by the volume of the cell (V_c), i.e.:

$$P_c = \sum_{i=1}^{N} \left(V_f\, P_f\right)_i / V_c \quad (2\text{-}6)$$

The intersecting volume of the fracture f may be written as:

$$V_f = L_f\, W_f\, b_f \quad (2\text{-}7)$$

where L_f, W_f and b_f denote the physical dimensions (length, width and thickness) of the intersecting fracture in three orthogonal directions. For the sake of simplicity, it is assumed in the equations below that the fracture thickness b_f is much thinner than the geometrical resolution of the computational grid (the grid size).

Grid-cell hydraulic conductivity

DarcyTools assumes that fracture transmissivity (T_f) is a scalar quantity and that fracture hydraulic conductivity (K_f) may be written as:

$$K_f = T_f / b_f \quad (2\text{-}8)$$

where b_f *is* the fracture thickness. Thus, the contribution from an intersecting fracture to the hydraulic conductivity of the intersected grid cell may be written as:

$$K_{c,f} = (L_f\, W_f\, T_f) / V_c \quad (2\text{-}9)$$

Since DarcyTools uses a staggered computational grid, $K_{c,f}$ is a directional quantity.

Grid-cell kinematic porosity

DarcyTools assumes that the kinematic porosity of a fracture (ϕ_f) can be written as:

$$\phi_f = e_{T,f} / b_f \quad (2\text{-}10)$$

where $e_{T,f}$ is the fracture transport aperture. Thus, the contribution from an intersecting fracture to the kinematic porosity of the intersected grid cell can be written as:

$$\phi_{c,f} = (L_f\, W_f\, e_{T,f}) / V_c \quad (2\text{-}11)$$

For the sake of clarity, it is emphasised that the stochastic fractures used in the work reported here are imported from the flow modelling of periods of temperate climate condition /Joyce et al. 2010/, see Section 3.5.

2.2.3 Particle tracking

The particle tracking routine, PARTRACK, has two modes of operation; the first is the classic way of moving the particle along the local velocity vector, while the second method uses the so called “flux-weighting” approach, and works as follows.

- A particle entering a scalar cell will, if no dispersion effects are activated, stay in the cell for a time which is equal to the free volume of the cell divided by the flow rate through the cell.
- When the particle is ready to leave the cell, it will leave through one of the cell walls that have an outgoing flow direction. The choice between cell walls with an outgoing flow is made with a likelihood that is proportional to the outflows. If several particles are traced, the cloud will thus split up in proportion to the flow rates. Complete mixing in a cell is assumed.

3 Model specifications

The hydrogeological conceptual model applied in this study was the Forsmark final site descriptive model, SDM-Site /SKB 2008/. If not stated otherwise below, the properties used are the same as those used by /Svensson and Follin 2010/ and they were imported from their DarcyTools model setup. The input file names and versions are specified in Appendix A.

In this study, the following changes and additions were made to the DarcyTools base case model setup imported from /Svensson and Follin 2010/:

- The flow-wetted surface of the bedrock was specified for sub-domains of the model according to the specification in /Vidstrand et al. 2010/ (Section 3.5 below).
- The size (side length) of grid cell at the tunnel walls of the repository, with the exception of deposition tunnels and deposition holes, was decreased from 4 m to 1 m (Section 3.6).
- No grouting was simulated, i.e. no restrictions were applied on the hydraulic conductivity of the grid cells in contact with the repository.
- Hydraulic and transport properties of backfilled repository parts (hydraulic conductivity, kinematic porosity, and flow-wetted surface) were set according to the reference closure as specified in /Joyce et al. 2010/ (Section 3.5 below).
- The density of the groundwater was fixed to fresh-water density, i.e. density variations were ignored.
- Due to the constant-density assumption, the head at the sea bottom was specified corresponding to fresh water density (Section 3.7). In the base case of /Svensson and Follin 2010/ the sea bottom boundary condition was corresponding to the salinity of the Baltic Sea.
- Tunnels that were open or backfilled with materials with a high hydraulic conductivity were simulated using internal specified-head boundaries in the tunnels (Section 3.2).
- For the glacial simulation cases, the boundary condition from the base case setup was replaced by a specified-head boundary at the top surface of the model (Section 3.7).

3.1 Studied cases

The hydraulic effects of a water-filled, partially open repository were studied for two different situations, a temperate situation with present-day boundary conditions and a generic future glacial situation with the ice front above the repository. For both these situations the case with a partially open repository was compared to the reference case with a closed repository, which gave the four studied cases listed in Table 3-1.

In contrast to the groundwater flow modelling of the excavation and operations periods reported in /Svensson and Follin 2010/, the work reported here concerns an abandoned partially open water-filled repository. The deposition tunnels are in all cases assumed to be backfilled and closed, but all other parts of the repository such as ramp, shafts, central area, access and transport tunnels are assumed to be left open in the open tunnels cases (Figure 3-1). All these repository parts are in this report collectively referred to as “tunnels”.

Table 3-1. Names of studied simulation cases.

Case	Explanation
	Temperate cases
(a)	Reference closure
(b)	Open tunnels
	Glacial cases
(c)	Reference closure
(d)	Open tunnels

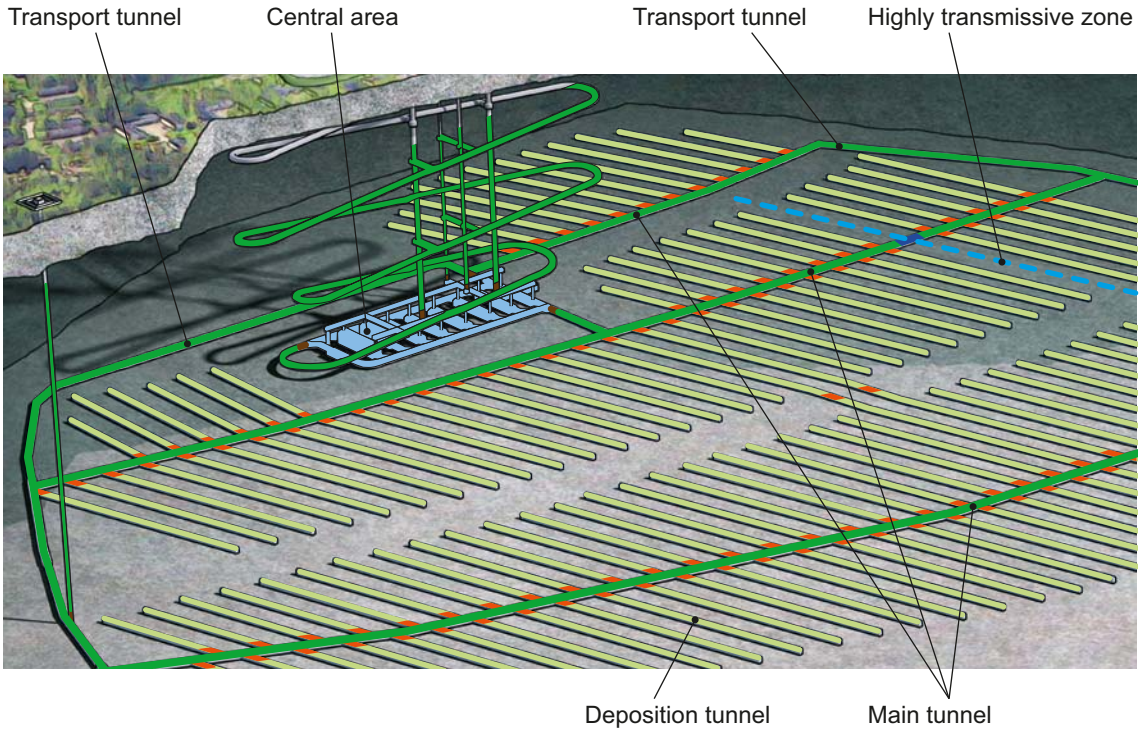

Figure 3-1. *Reference design for repository closure (Figure 3-1 in /SKB 2010a/). In the open tunnels cases it is assumed that only the deposition tunnels are backfilled and plugged towards the main tunnels.*

The present-day sea level was used for both the temperate cases and the glacial cases. During the temperate period, within the next 10,000 years, the Forsmark area is expected to be elevated approximately 40 m /Joyce et al. 2010/. Therefore also the sea, which is the downstream boundary, will be displaced and the hydraulic gradient in the area will change. The temperate case with the present-day sea level can be seen as a pessimistic case regarding the hydraulic effects of a partially open repository since the importance of open tunnels as easy path ways for groundwater flow between repository depth and the surface will decrease as the area undergoes a transition from a discharge area for deep groundwater to more of a recharge area.

The simulated glacial situation with the present-day sea level may be representative for an advancing ice sheet /Vidstrand et al. 2010/. The hydraulic gradient through the repository is high, with recharge behind the ice front and discharge immediately ahead of the ice. The hydraulic conditions prevailing at the end of the temperate period at about year 12,000 AD may be somewhere between the conditions at these two extremes.

No calibration of the model was done in this study since that was outside the scope of work. The hydraulic properties of the deformation zones and the properties of the hydrogeological DFN have been done within the site descriptive modelling. As regards the Forsmark DarcyTools model, the near-surface part of the basic model setup has been calibrated to some degree by /Svensson and Follin 2010/ and in earlier studies.

3.2 Methodology for simulation of tunnels

3.2.1 Backfilled tunnels

In the reference closure cases all tunnels were backfilled whereas only the deposition tunnels were backfilled in the open tunnels cases. Backfilled tunnels were simulated by the assignment of specified hydraulic conductivity values to the grid cells inside tunnels (see Chapter 3.5). The exception to this method of simulating backfilled tunnels is that, when simulating the reference closure cases, some backfilled repository features with a relatively high hydraulic conductivity had to be handled differently for numerical stability reasons.

The first of these features are the parts of the repository above an elevation of –200 m (RHB 70), i.e. the upper parts of the ramp and shafts, where a top sealing hydraulic conductivity of $1.0 \cdot 10^{-1}$ m/s should be applied according to the specifications in /Joyce et al. 2010/. These parts correspond to the zone of the repository where the backfill could be degraded by permafrost. Instead of assigning a hydraulic conductivity, a specified-head boundary condition was applied in the top sealing parts. The motivation for this is that due to the large contrast in hydraulic conductivity between the tunnel and the surrounding rock, because of the large hydraulic conductivity of the degraded backfill, the hydraulic gradient inside the tunnel should be negligible. Further, the backfilled repository parts exiting at the surface are in contact with transmissive surface layers and they are thus assumed to not influence the hydraulic head at the surface. Therefore, a constant head representing the simulated undisturbed head in the surface layer at their respective exit point (Figure 3-2) was applied to the upper parts of the ramp and the shafts (Table 3-2). The specification of the boundary condition at the surface in the glacial case is described in Section 3.7 below.

The second repository feature handled differently is the central area tunnels where a hydraulic conductivity of the backfill of $1.0 \cdot 10^{-5}$ m/s should be applied according to the specifications /Joyce et al. 2010/. Due to the large hydraulic-conductivity contrast between the tunnels and the surrounding rock a lower conductivity had to be applied in the central area tunnels for numerical stability reasons. If the conductivity of the tunnel backfill is large, an increased conductivity of the backfill will not give a much larger flow, as the flow is mainly dependent on the conductivity of the surrounding rock mass. Thus, a threshold conductivity can be defined which is the smallest conductivity that could represent the conductivity of a high-conductive backfilled (or open) tunnel that is closed at its ends /Holmén 1997/. The threshold conductivity for a tunnel was calculated by /Holmén 1997/ to be of the order of 100–1,000 times the conductivity of the surrounding rock depending on the length of the tunnel and the direction of the tunnel in relation to the direction of the regional flow. Since the conductivity of the rock surrounding the central area of the repository is of the order of $1.0 \cdot 10^{-10}$ m/s, a conductivity of $1.0 \cdot 10^{-7}$ m/s was regarded to be sufficient to represent the high-conductive backfill in the central area.

Table 3-2. Specified head in top sealing repository features above an elevation of –200 m (RHB 70) applied in the temperate and glacial cases with reference closure of tunnels.

Repository feature	Specified hydraulic head [m]	
	Temperate	Glacial
Ramp	0.1	220.0
Shafts central area	0.1	220.0
West deposition area ventilation shaft	1.8	123.0
East deposition area ventilation shaft	0.2	4.0

3.2.2 Open tunnels

For the simulation of open tunnels an approach with specified head in the open tunnels was chosen of numerical stability reasons. The EPANET 2 pipe network model /Rossman 2000/ was used for coping calculations of the flow through the open tunnel system during present-day conditions and for calculation of the head distribution in the open tunnels for the glacial case that subsequently was used as a specified-head boundary condition in DarcyTools as described below.

There is a high capacity for flow through the open repository tunnel system. Therefore, for the present-day boundary conditions with a relatively low hydraulic head difference between the inlet and outlet points, it is the supply of groundwater from the transmissive soil layer at the inlet points that limits the flow through the tunnel system. This was confirmed by scoping simulations using the EPANET 2 pipe network model. For all realistic flows through the system, the head loss along the tunnels will be very small. A constant head equal to the drainage level of the tunnel system was therefore applied to all open tunnels for the temperate situation. The drainage level was assumed to be equal to the lowest simulated undisturbed head in the soil layer at the outlets from the repository which was 0.07 m at the shafts above the central area (Figure 3-2).

For the glacial case the flow through the open tunnel system is governed by the head difference over the tunnels and the friction losses in the tunnels. For the specified boundary conditions (see Chapter 3.7) there will be a considerable flow through the tunnel system, and the head losses along the tunnels and in bends, tunnels crossings etc. will be significant and irregularly distributed through the tunnel system. The EPANET 2 pipe network model was used to calculate the head distribution in the tunnels. The simplified model of the tunnel system that was implemented in EPANET 2 is shown in Appendix B. The geometry of the repository (tunnel lengths, diameters and connectivity structure) was taken from provided CAD files (see Appendix A). A hydraulic roughness of 0.3 m was assumed for blasted tunnels and 0.02 m for raise-drilled shafts and ducts. Minor head losses were accounted for at exits, enlargements and contractions, crossings and sharp bends.

In the glacial case all openings of the repository are below the ice sheet except for the eastern ventilation shaft in the deposition area. With the specified top boundary condition (Chapter 3.7) the flow through the tunnel system at repository level was estimated to be about 250 m^3/s which is a huge flow. The flow in relation to the availability of water below the ice sheet is further discussed below in Section 5.2. The major head losses occur in the relatively narrow ventilation shafts in the deposition area (Figure 3-3) where the outflows take place (Table 3-3). From the calculated head distribution a constant head was assigned to the open tunnels in a number of sections according to Table 3-4.

Table 3-3. Distribution of flow in to and out from the repository level for the glacial case calculated by EPANET 2.

Repository feature	Relative flow [%]
Inflow	
Hoist shaft	36
Skip shaft	28
Air intake shaft	16
Ramp	13
Air exhaust shaft	7
	100
Outflow	
East deposition area ventilation shaft	61
West deposition area ventilation shaft	39
	100

Table 3-4. Specified head in open tunnels applied in the glacial case.

Repository feature	Specified hydraulic head [m]
Ramp and shafts above central area	220
Central area and tunnels North West	215
Tunnels South East	200
West deposition area ventilation shaft	linear decline from 200 at repository level to 123 at surface
East deposition area ventilation shaft	linear decline from 200 at repository level to 4 at surface

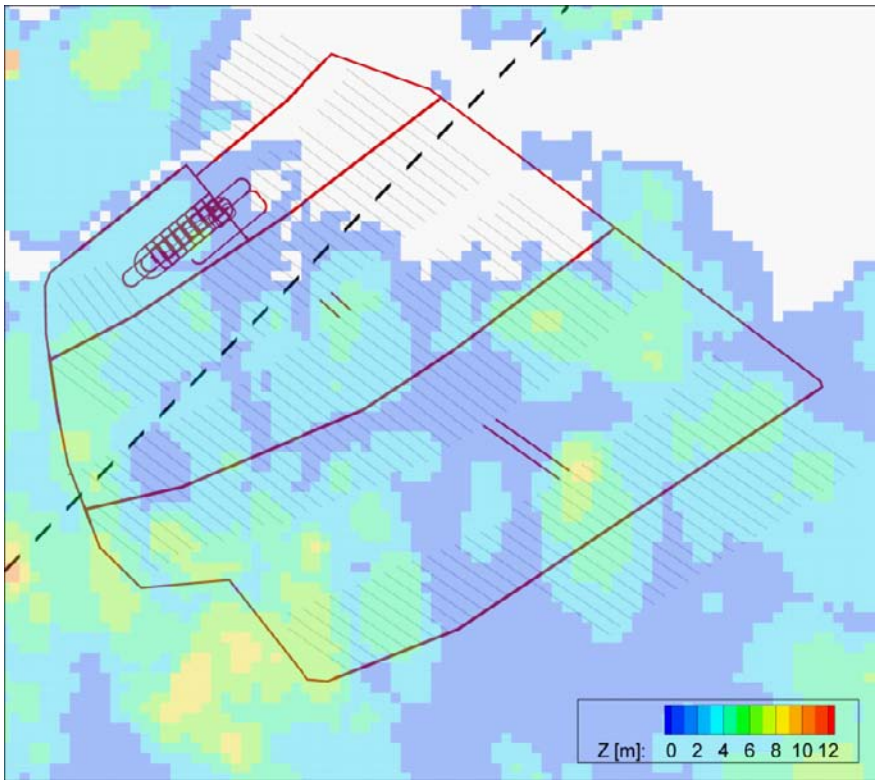

Figure 3-2. *The modelled topography above the repository. White areas are below sea level (0 m RHB 70). For present-day boundary conditions the flow through the open tunnel system is from the two ventilation shaft inlets in the deposition area to the outlets of the ramp and shafts above the central area at a lower level. Depositions tunnels are coloured in grey, all other repository features are coloured in red. The dashed line indicates the location of the ice front in the glacial cases.*

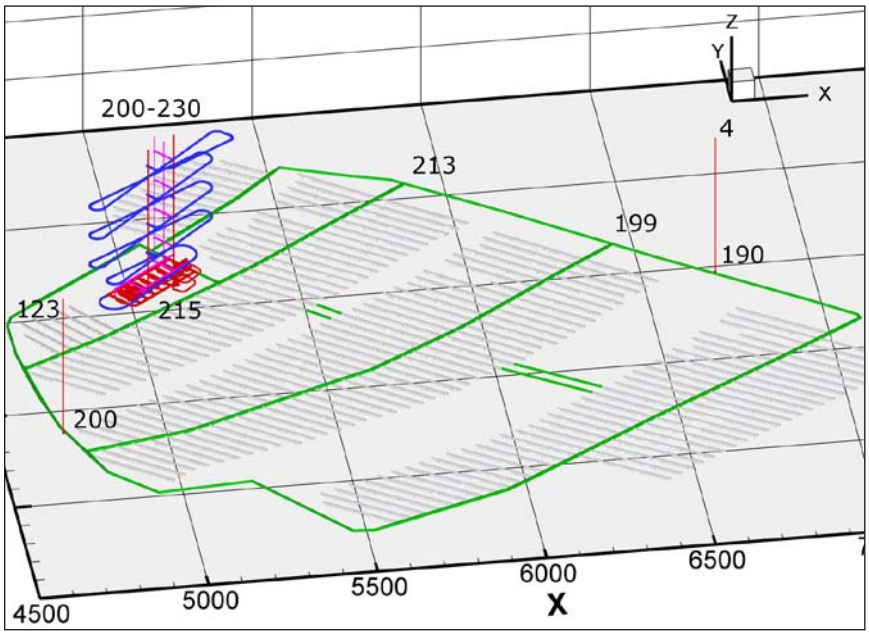

Figure 3-3. *Schematic illustration of the head distribution (in meter above sea level) in the open tunnel system for the glacial case calculated by EPANET 2.*

3.3 Performance measures

The results of the simulations are shown as fields of hydraulic head and Darcy flux at repository depth and as the difference in those variables between the reference cases and the open tunnel cases. Moreover, the distribution of flow in to and out from open tunnels are illustrated and numbers are given on the total flow in and out.

The specific performance measures of the results from this study are the distributions (empirical cumulative distribution functions, CDF) of Darcy flux at the deposition positions and advective travel time and the flow-related transport resistance (F-factor) for particles travelling from the deposition positions to surface. In addition, also the distribution of flow-path length of the particles is reported.

The CDF of Darcy flux was estimated from all released particles, i.e. it sums up to 100%, whereas the CDFs of advective travel time, F-factor and flow-path length only include the particles that had reached surface at the end of the simulation, i.e. they do not necessarily sum up to 100%. A particle entering an open tunnel or the top sealing of the repository was assumed to reach surface directly, and hence all particles reaching surface, either via flow paths in the bedrock or via tunnels, were included in the statistics. The median of the F-factor and flow-path length reported below were estimated from the particles reaching surface. On the other hand, all released particles were included in the calculation of median advective travel time since it is known the particles not yet at surface at the end of the simulation have longer travel times.

3.4 Model domain

The model domain was the same as the regional domain used for groundwater flow modelling in the Site Descriptive Modelling (SDM). The dimensions of the domain, outlined in Figure 3-4, were about 15 km (north-south), 10 km (west-east), and 1.2 km (depth). The boundary of the model domain follows the topographical water divide in south-west and then strikes parallel to the direction of flow towards the sea.

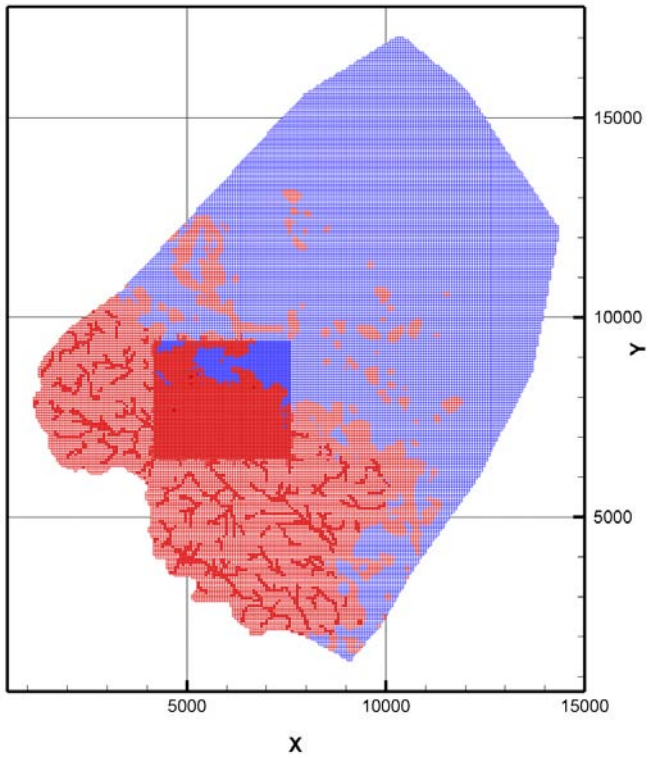

Figure 3-4. *Top view of the model grid. Red-shades areas are land-surface cells and the blue-shaded areas area sea-surface cells. The repository site is the refined rectangular area. Streams are visible as a network of refined cells.*

A local coordinate system was used in this study (Figure 3-4), where (X (E), Y (N)) = (0, 0) in the local system corresponds to (1626000, 6692000) in the Swedish national RT 90 system. The Z-coordinate (elevation) is given in the national RHB 70 levelling system.

3.5 Hydraulic properties

The geometry and hydraulic properties of deformation zones, sheet joints, and the stochastic discrete fracture network (DFN) were the same as in the SDM work. The values of these properties and a realisation of the DFN was imported from the base case of the groundwater flow modelling by /Joyce et al. 2010/.

A soil cover was not explicitly modelled. Instead a more permeable and porous surface layer was modelled to a depth of 20 m below the surface (land or sea bottom). In this layer a constant vertical hydraulic conductivity of $1 \cdot 10^{-6}$ m/s was applied, whereas an exponential depth decrease was used for the horizontal hydraulic conductivity:

$$K = 5 \cdot 10^{-3}\ 10^{-d/(3\ \mathrm{m})}\ \mathrm{m/s} \qquad (3\text{-}1)$$

where d is the depth below surface. A minimum horizontal hydraulic conductivity of $1 \cdot 10^{-7}$ m/s was also applied in this layer. A similar relation was used for the kinematic porosity n:

$$n = 5 \cdot 10^{-2}\ 10^{-d/(20\ \mathrm{m})} \qquad (3\text{-}2)$$

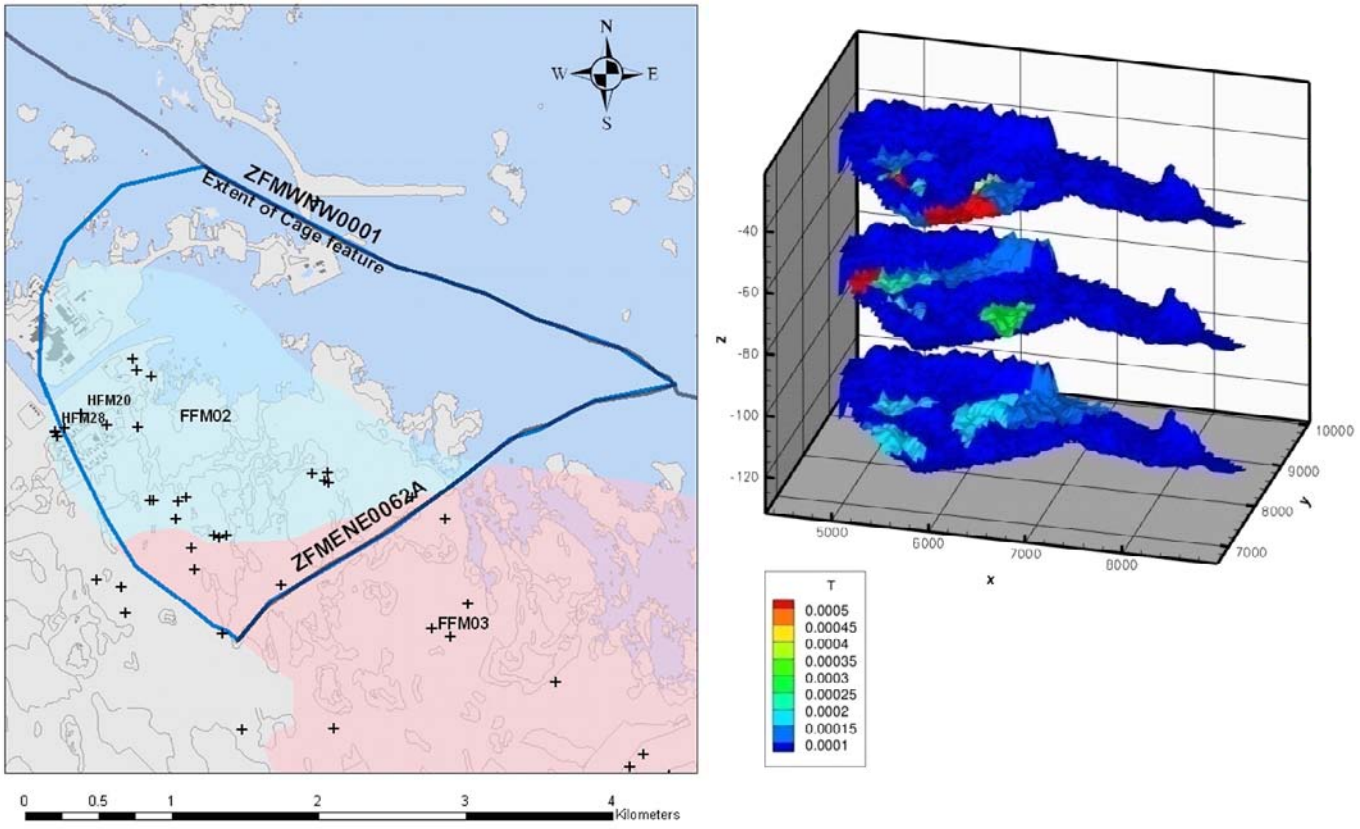

Figure 3-5. *The hypothesised lateral extent (left) and elevations (right) of the discrete features modelled to represent the sheet joints observed in the shallow bedrock aquifer in the SDM work. The crosses in the left image mark the positions of percussion- and core-drilled boreholes for which transmissivity measurements were available. The bluish/greenish area in the upper image represents fracture domain FFM02 and the pinkish area represents fracture domain FFM03. (Figure 5-17 in /Follin 2008/.)*

Grid cells that were in contact with the defined network of streams (Figure 3-4) were given a high horizontal hydraulic conductivity ($K = 2 \cdot 10^{-1}$ m/s). The same stream network was in the simulations of both temperate and glacial conditions.

The hydraulic conductivity fields within the fracture domains were derived from the transmissivities of the fractures of the imported stochastic DFN using the upscaling methodology in DarcyTools described in Section 2.2.2. Below the surface layer, inside the fracture domains, a minimum hydraulic conductivity of $1 \cdot 10^{-10}$ m/s was applied to the bedrock. In the bedrock outside the fracture domains (outside deformation zones) a hydraulic conductivity of $1 \cdot 10^{-7}$ m/s was applied in the upper 200 m below the ground surface (below the surface layer), $1 \cdot 10^{-8}$ m/s in the depth interval 200–400 m below the ground surface, and $3 \cdot 10^{-9}$ m/s below 400 m.

Advective transport was considered in this study. The kinematic (transport) porosity was therefore implemented in the model. Also the flow-wetted surface was implemented in order to calculate flow-related transport resistance for the particle flow paths. The kinematic porosity was derived from the underlying deformation zone model and the DFN according to /Svensson and Follin 2010/, and a minimum value of $5 \cdot 10^{-5}$ was used both inside and outside the fracture domains. The flow-wetted surface was specified for each individual fracture domain and depth interval according to the specification in /Vidstrand et al. 2010/.

The values of the hydraulic properties of the backfilled tunnels (Figure 3-1) were also imported from the work by /Joyce et al. 2010/. A hydraulic conductivity of $1 \cdot 10^{-10}$ m/s and a kinematic porosity of 0.45 was used for all backfilled tunnels except from in the top sealing of the repository and the central area tunnel that was treated differently, see Chapter 3.2.1. In the central area tunnel the kinematic porosity was set to 0.27. Note that according the specifications the flow-wetted surface was assumed to be zero in all tunnels, backfilled as open. The same properties were used for the deposition holes as for the deposition tunnels.

3.6 Computational grid

The model domain described in Section 3.4 was discretized by an unstructured grid built by the grid generation program within DarcyTools /Svensson et al. 2010/. The basic discretization applied was a cell size (side length) of 128 m in both horizontal and vertical direction. The grid was then further refined in different part of the domain according to Table 3-5 (Figure 3-4). A description of the grid generation process in DarcyTools and the possible setting is found in /Svensson et al. 2010/. The resulting grid contained about 3.2 million cells.

3.7 Initial and boundary conditions

A steady-state model does not strictly require initial conditions. However, as the method of steady-state simulation in this study was time stepping towards a pseudo steady-state, initial conditions had to be specified. Also, the initial conditions will affect the numerical stability and convergence properties of the model. The initial condition for the reference simulations with a closed repository was a vertical hydrostatic equilibrium, with the water table at a specified depth below ground surface. The steady-state pressure distributions from the reference simulations were then used as initial condition for the simulations with open tunnels.

For the temperate cases, the boundary conditions from the original model setup by /Svensson and Follin 2010/ were used. The lateral boundaries of the model domain consisted of water divides and a no-flow boundary was thus applied. A no-flow boundary was also applied at the bottom of the model. For the land-surface cells a flux equal to the estimated net precipitation of 130 mm/yr was specified /Svensson and Follin 2010/. The position of the free water table is calculated by DarcyTools in an iterative manner /Svensson et al. 2010/. A hydrostatic pressure equal to the water depth was applied to the sea bottom cells.

The same boundary conditions were maintained for the glacial cases as for the temperate cases, except for the boundary condition at the top-surface cells. An ice sheet with the ice front above the repository was simulated in the glacial cases, see Figure 3-2. The coordinates of the ice front was those of the ice front location "IFL II" in /Vidstrand et al. 2010/. On the top surface below the ice sheet the groundwater pressure was set equal to the weight of the overlying ice, see the discussion of glacial conditions in /Vidstrand et al. 2010/. The ice sheet elevation was calculated as a function of the distance (x) from the ice sheet centre by the expression /Vidstrand et al. 2010/:

$$h(x) = H\left(1 - \left(\frac{x}{L}\right)^{\frac{4}{3}}\right)^{\frac{3}{8}} \qquad (3\text{-}3)$$

where the ice thickness at the ice sheet centre, H, was 3,000 m, and the length of the ice sheet, L, was 400 km.

Ahead of the ice front, atmospheric pressure was applied to the land surface, and the present-day sea level was maintained.

The internal boundary conditions in open tunnels and in the top sealing of the repository in the reference closure cases are explained in Chapter 3.2 above.

Table 3-5. Requirements on the grid resolution.

Grid element	Horizontal resolution [m]	Vertical resolution [m]	Cross 2:1 rule (Y/N)	Long. 2:1 rule (Y/N)
Base	128	128	Y	N
Top surface	64	2	Y	N
Rivers	32	2	Y	Y
Repository area	32	32	Y	Y
Deposition tunnels	4	4	Y	Y
Repository features, other	1	1	Y	Y

3.8 Transport simulation

Particle tracking was performed in order to study the flow paths from the deposition holes to surface and to calculate the transport performance measures (Chapter 3.3). One particle was released at each of the specified 6,916 deposition holes. The modelled hydraulic conductivity in the deposition holes was low ($1 \cdot 10^{-10}$ m/s) and the porosity was quite high (0.45), and hence the advective flow through the deposition holes will be extremely slow. Since it was the transport in the bedrock and not in the engineered barriers inside the deposition holes that was of interest here, the particles were released some distance outside the deposition holes to avoid grid cells with deposition hole hydraulic properties. The release points were located 4 m below the deposition tunnel floor, and due to the 4 m grid resolution at the deposition tunnels the particle starting points were moved 5.5 m in the X- and Y-directions from the centre line of the deposition holes.

The traditional particle tracking method by moving the particle along the local velocity vector was employed. The particles were tracked for a simulation time of at least 475,000 years. It should be emphasized that the particle tracking was done in the steady-state flow field, i.e. the flow field does not change with time. In reality, the flow field will change, especially at the ice front. The time independent flow field is an important assumption, especially for the particles with long breakthrough times.

The particles that entered open tunnels, or the permeable top sealing of the repository in the reference closure case, during the particle tracking were captured at the point of entry. The particle was assumed to reach surface immediately at the entry in the tunnel, i.e. the flow-path length, advective travel time and transport resistance between the point of entry in the tunnel and surface were assumed to be zero, and the particles that entered tunnels were included in the total transport statistics.

3.9 Numerical solution

The steady-state solutions were sought by time stepping towards a steady state. The simulations were ended when the residuals had decreased several orders of magnitude and levelled out, and when heads and fluxes had converged. The relative change in the variables at the monitored control points in the model were in all cases less than 0.001 per year at the end of the simulations.

The total mass balance was calculated for a control volume surrounding the repository at repository level for the reference closure cases. The mass imbalance was smaller than some per mille of the total flow through the control volume.

4 Results

4.1 Temperate cases

4.1.1 Hydraulic head

The simulated hydraulic gradient at repository depth for the present-day conditions is from south-west to north-east (Figure 4-1). The hydraulic gradient virtually vanishes at the present coast line. The effect of the open tunnels is visible as a drawdown around the tunnels in the western part of the repository (Figure 4-1) that causes a hydraulic gradient towards the open tunnels. The maximum radius of influence around the tunnels is about 300 m (Figure 4-1 lower) and the maximum drawdown, i.e. the difference in head between the reference closure case and the open tunnel case, is about 2 m at the tunnels in south-west.

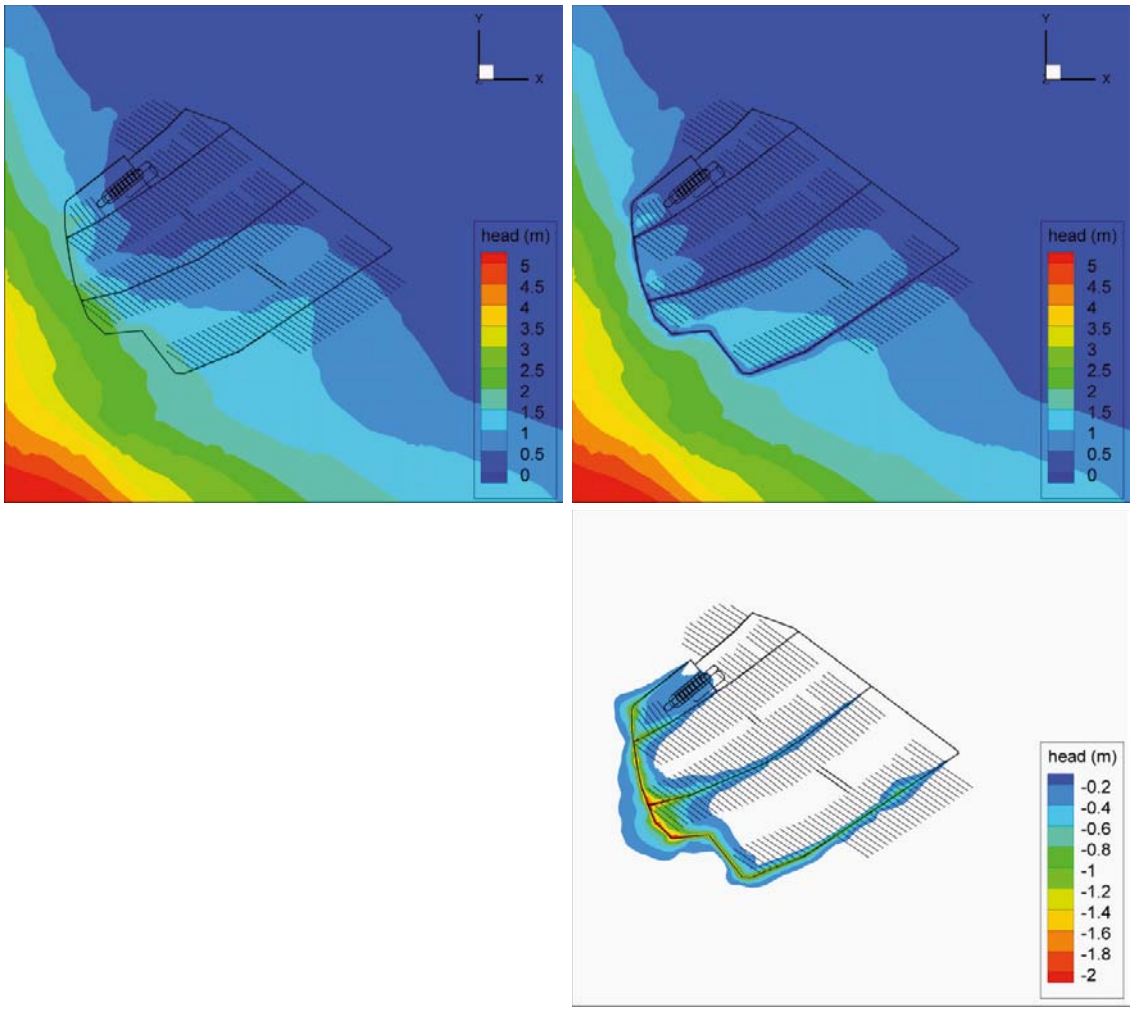

Figure 4-1. *Hydraulic head field at repository depth (Z = –465 m RHB 70) during temperate conditions for the reference closure case (upper left) and the open tunnel case (upper right). The datum level for head is 0 m RHB 70. The change in hydraulic head caused by the open tunnels is shown in the lower right image.*

4.1.2 Flow

The effect of the open tunnels at repository depth is apparent as an increased flux in the nearest surroundings of the tunnels, and locally in the deformation zones in contact with the tunnels (Figure 4-2 and Figure 4-3). An effect of larger spatial extent, although small in magnitude, can be seen in the southernmost part of the repository, where there is an increased flux. On the other hand, a decreased flux can also be seen downstream the open tunnels in some areas. The vertical component of the flux at repository depth is changed significantly only locally in the deformation zones in contact with the open tunnels (Figure 4-3 and Figure 4-4).

The distribution of flow between the open tunnels and the surrounding rock or soil is shown in Figure 4-5. The general pattern of flow is inflow to the ventilation shafts in the deposition area and discharge through the ramp and shafts above the central area. The calculated total inflow, from soil and rock, to open tunnels is 0.42 L/s and the outflow to the surrounding bedrock is $2 \cdot 10^{-3}$ L/s. The surface layer and the sheet joints that were crossing the shafts and the ramp are dominating the flow into the tunnel system.

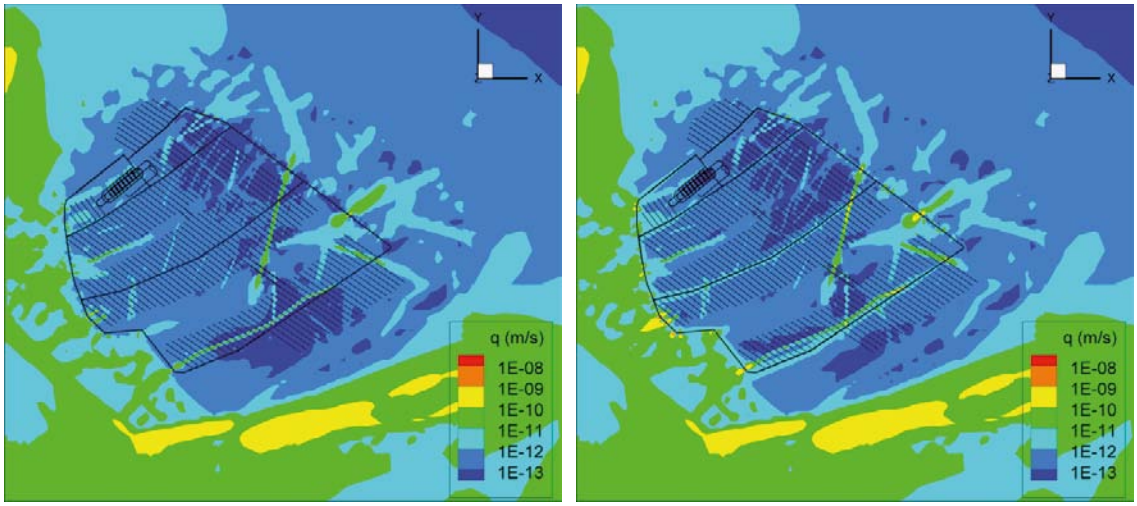

Figure 4-2. *Darcy flux magnitude at repository depth (Z = –465 m RHB 70) during temperate conditions for the reference closure case (left) and the open tunnel case (right).*

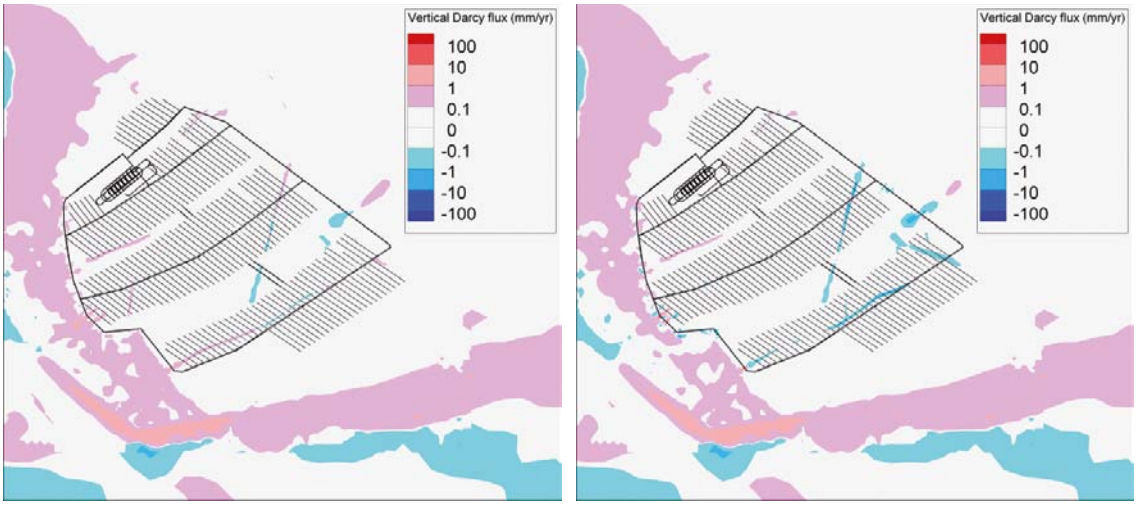

Figure 4-3. *Vertical Darcy flux in mm/yr at repository depth (Z = –465 m RHB 70) during temperate conditions for the reference closure case (left) and the open tunnel case (right). Positive flux is directed upwards.*

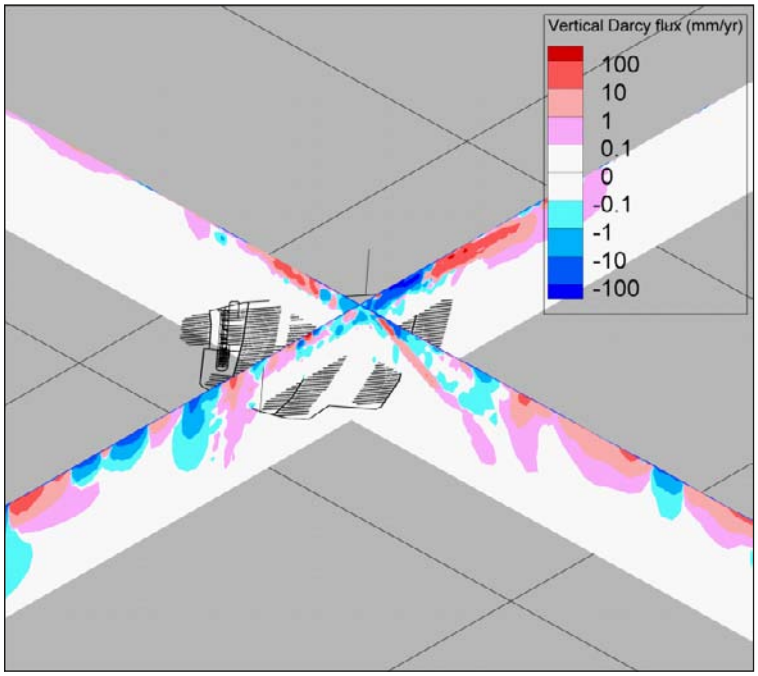

Figure 4-4. *Vertical Darcy flux in mm/yr during temperate conditions for the open tunnel case. View from south-west. Positive flux is directed upwards.*

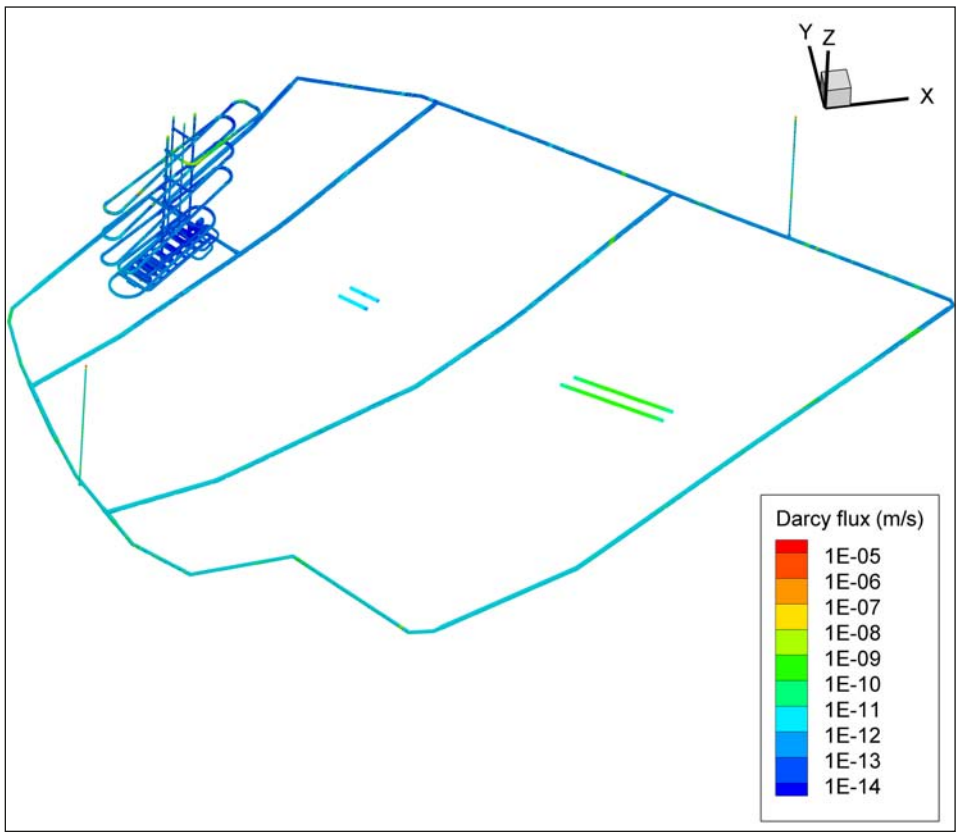

Figure 4-5. *Magnitude of Darcy flux between open tunnels and the surroundings during temperate conditions.*

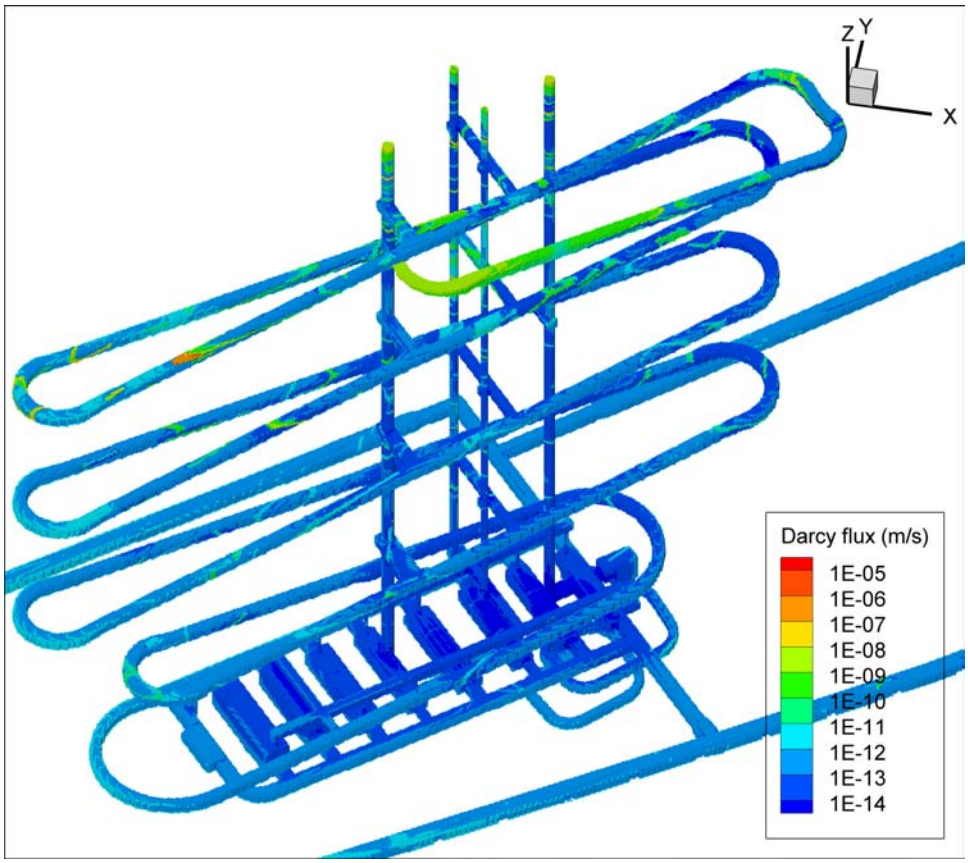

Figure 4-6. *Close-up view of the central area of the repository showing the magnitude of simulated Darcy flux between open tunnels and the surroundings during temperate conditions.*

Since the calculated outflow from the open tunnels to the surrounding bedrock is very small, the discharge through the ramp and the shafts to the surface above the central area could be estimated as the sum of inflow to the tunnels. The discharge, which is equal to the maximum flow through the tunnel system, could thus be estimated to 0.42 L/s, where 0.26 L/s emanates from the transmissive surface layer and sheet joint above Z = –40 m (RHB 70).

The effect on the total turnover of groundwater in the rock volume containing the repository (below Z = –40 m) was also studied. This was done by defining a rectangular control volume (box) that surrounded the repository, with the upper face of the control volume located at the elevation –40 m. The extent of the control volume in the horizontal plane corresponds approximately to the area of grid refinement visible in Figure 3-4. The change in the total flow through this bedrock volume was then calculated. The sum of inflow over the outer boundary of the volume changed from 2.81 L/s to 2.86 L/s, i.e. an increase of about 2%.

4.1.3 Particle trajectories and discharge locations

The simulated discharge locations for the particles that reached the surface are shown in Figure 4-7 (tracking time 475,000 years in the reference case and 790,000 years in the open tunnel case). In this figure, only particles that reached the surface through flow paths through the bedrock are shown; the particles that enter open tunnels, or the top sealing of the repository in the reference case, during the particle tracking are captured at the point of entry. When a particle entered a tunnel it was assumed to reach surface directly, and hence all particles reaching the surface via flow paths in the bedrock or via tunnels were included in the particle tracking statistics. The general direction of flow from south-west to north-east is apparent. All surface discharge points are located outside the coast line since the land surface was modelled as a recharge boundary. In the reference closure case, about 75% of the

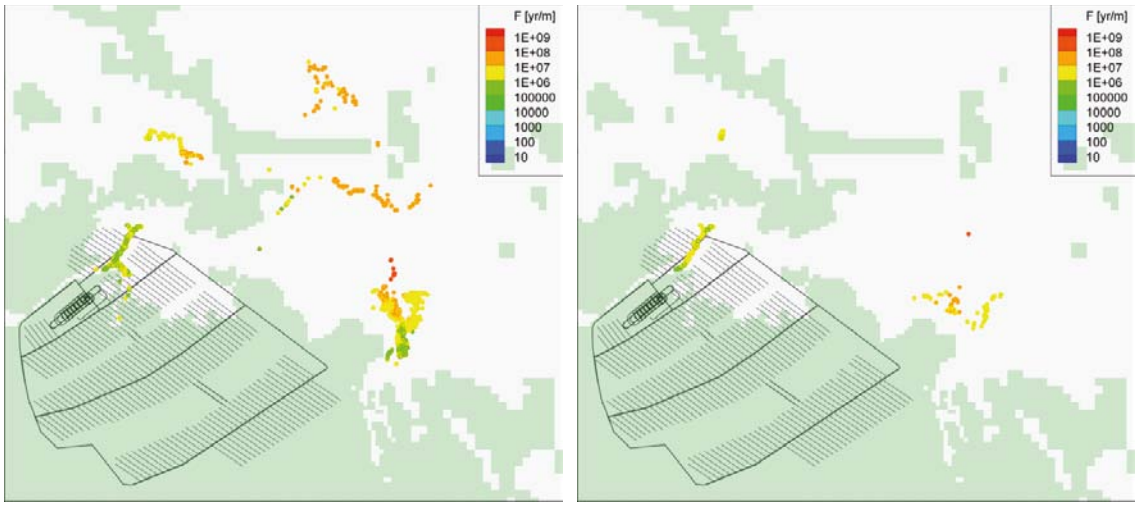

Figure 4-7. *Discharge locations at surface for particles released at the 6,916 deposition hole positions during temperate conditions for the reference closure case (left) and the open tunnel case (right). The exit points are coloured by the flow-related transport resistance (F-factor) for the flow path. The locations of the particles that entered open tunnels are not shown.*

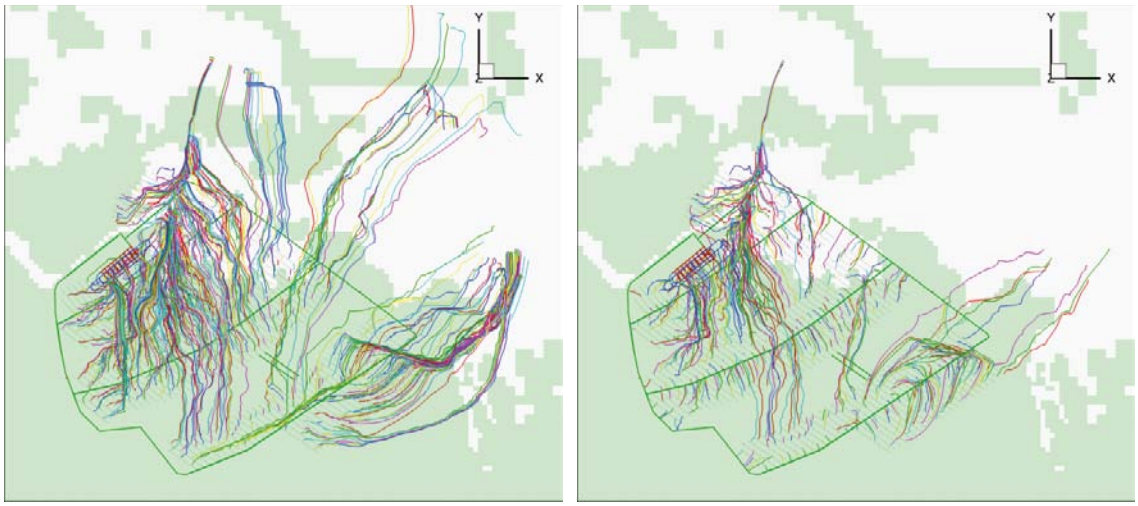

Figure 4-8. *Horizontal projection of trajectories for particles released at 500 of the 6,916 deposition hole positions during temperate conditions for the reference closure case (left) and the open tunnel case (right).*

particles from the 6,916 deposition positions reached the surface via flow paths entirely within the bedrock, whereas in the open tunnel case the majority of the particles discharged through the tunnels system (and thus not shown in Figure 4-7), and only about 20% reached the surface through flow paths entirely within the bedrock. The most apparent effect of the open tunnels is that the longest flow paths with the highest F-factors disappeared, but also some of the discharge points closest to the repository disappeared.

The full particle trajectories for 500 randomly chosen starting positions out of the 6,916 deposition holes are illustrated in Figure 4-8. The same starting positions for output of trajectories for plotting were used in all simulation cases. The flow towards open tunnels at repository depth is apparent; particles from many deposition hole positions travel to the nearest open tunnel in the open tunnel case.

4.1.4 Discharge performance measures

As already shown in Figure 4-2, the change in Darcy flux magnitude at the deposition hole positions due to open tunnels are quite small. The median flux increased from about $5.1 \cdot 10^{-6}$ m/yr ($\approx 1.6 \cdot 10^{-13}$ m/s) for the reference case to about $5.7 \cdot 10^{-6}$ m/yr for the open tunnel case, i.e. an increase of about 13% (Figure 4-9). The open tunnels do not significantly influence the spread of the flux distribution, but have a slight smoothening effect.

In the reference case, in total 88% of the particles reached surface (Figure 4-10). The particles that entered the top sealing of the repository and reached surface through the uppermost parts tunnels were 13% of the total number of released particles. In the open tunnel case, in total 92% of the particles reached surface, but 72% discharged through the open tunnels.

The flow-path lengths in the reference case are distributed between approximately 400 m and 4,100 m, with the median (calculated from the flow paths of the particles discharged at surface) at about 1,300 m (Figure 4-10). The flow-path length must be longer than or equal to the Euclidian distance between the release point and the nearest possible discharge point. The shortest flow-path lengths correspond to particles that discharged through the top sealing of the repository, and the shortest flow-path length through bedrock is approximately 600 m.

Open tunnels caused a drastic reduction in flow-path lengths. The shortest flow path is in this case about 10 m and the longest about 2,500 m, with the median (calculated from the flow paths of the particles discharged at surface) at about 200 m. Also in this case, the shortest flow path through bedrock to surface is about 600 m, i.e. all shorter flow paths are to open tunnels. As displayed in the map of discharge locations on surface (Figure 4-7), an effect of open tunnels is that the longest flow paths (> 2,500 m) disappeared.

The advective travel time to surface for the fastest particles in the reference case is 60 yr, with the median (including all released particles) at about 2,700 yr (Figure 4-11). Similar to the transport length, the particles with shortest travel time discharged through the top sealing of the repository. The effect of the open tunnels is that a number of particles with a very short advective travel time appeared. The shortest travel time is 1.5 yr. This path, as an example, is from a deposition hole close to a transport tunnel. The deposition position is located within a (stochastic) structure with relatively high transmissivity and flow compared to the surrounding rock. The path goes via the structure to the nearby transport tunnel, with a path length of about 19 m. This path also has one of the shortest path lengths. It is visible in Figure 4-8 (right) that the shortest paths generally are from deposition holes close to transport tunnels to the open tunnel.

However, the overall travel time distribution is not that different from the reference case, and the median travel time is similar, about 2,300 yr (15% decrease). The travel time of the majority of the paths through bedrock to surface is between 1,000 and 10,000 yr.

The values of the flow-related transport resistance (F-factor) are above $1 \cdot 10^5$ yr/m in the reference case, with the median (calculated from the flow paths of the particles discharged at surface) at about $2 \cdot 10^6$ yr/m (Figure 4-12). The open tunnels decreased the median transport resistance to about 30% of the reference value. The open tunnels also caused a number of flow paths with very low flow-related transport resistance, down to approximately $2 \cdot 10^2$ yr/m. These flow paths are relatively short paths ending in open tunnels at repository depth, and they are associated to structures with high Darcy flux.

One noteworthy observation is that the remaining particles in the open tunnels case, particles that not entered tunnels, have longer minimum flow-path length, longer minimum advective travel time, and higher minimum F-factor compared to the reference case. This is not that surprising since the shortest flow paths that discharge closest to the repository can be expected to be most affected by the drawdown when the tunnels are kept open. However, the difference is not as large as it looks in the figures; there are some remaining particles in the open tunnels case with relatively short travel time and small F-factor that are not visible in the scale of the figures.

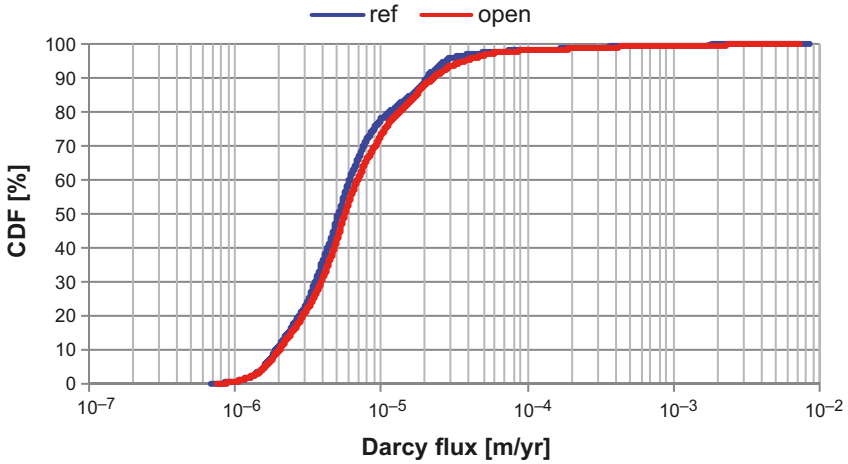

Figure 4-9. *Cumulative density function of simulated Darcy flux at the 6,916 deposition hole positions during temperate conditions for the reference closure case (blue) and the open tunnel case (red).*

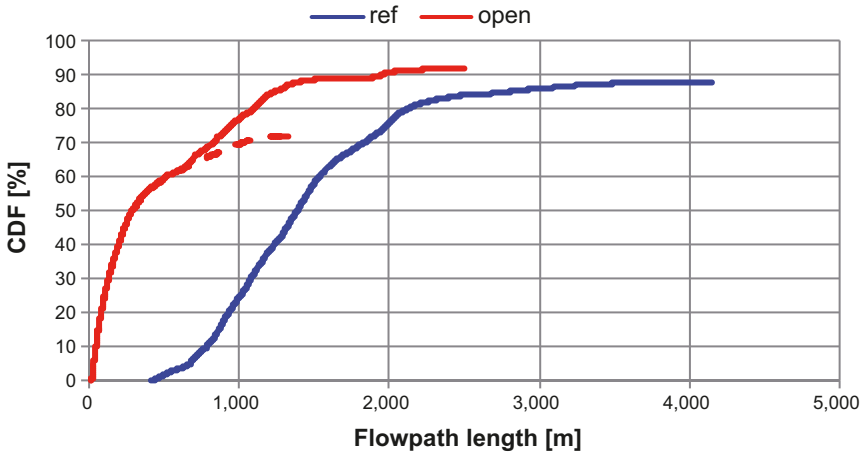

Figure 4-10. *Cumulative density function of simulated flow-path length for particles released at the 6,916 deposition hole positions during temperate conditions for the reference closure case (blue) and the open tunnel case (red). The solid red line represents all particles that reached surface and the broken red line represents the fraction of these particles that entered open tunnels.*

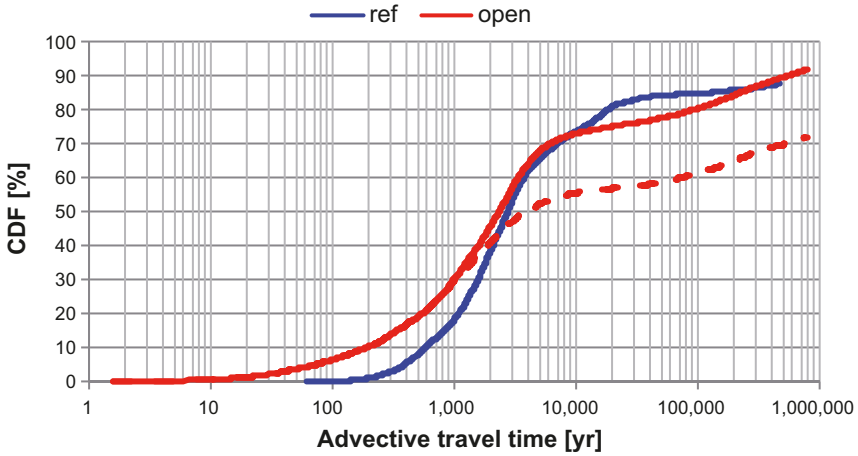

Figure 4-11. *Cumulative density function of simulated advective travel time for particles released at the 6,916 deposition hole positions during temperate conditions for the reference closure case (blue) and the open tunnel case (red). The solid red line represents all particles that reached surface and the broken red line represents the fraction of these particles that entered open tunnels.*

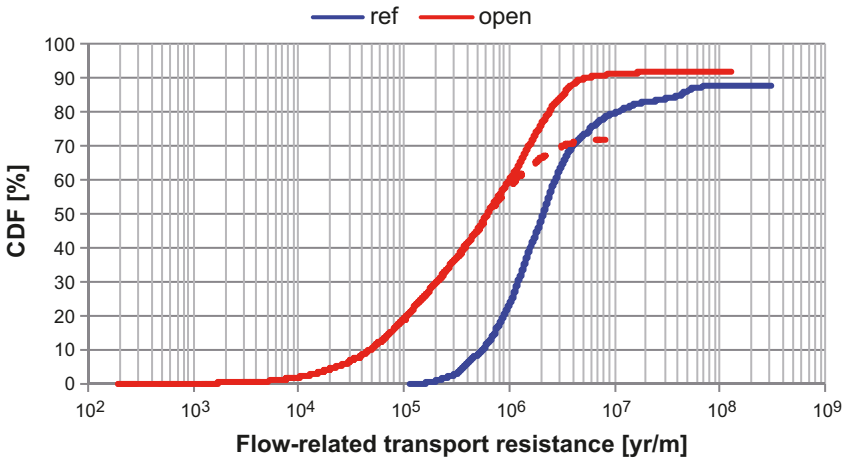

Figure 4-12. *Cumulative density function of simulated flow-related transport resistance (F-factor) for particles released at the 6,916 deposition hole positions during temperate conditions for the reference closure case (blue) and the open tunnel case (red). The solid red line represents all particles that reached surface and the broken red line represents the fraction of these particles that entered open tunnels.*

4.2 Glacial cases

4.2.1 Hydraulic head

Due to the applied glacial top boundary condition, with the ice front above the repository (the so called IFL II), the simulated hydraulic gradient at repository depth is directed from north-west to south-east (Figure 4-13). The gradient is thus rotated approximately 90° clockwise in relation to the present-day conditions. The gradient is strong below the ice sheet directly behind the ice front and it decreases rapidly ahead of the front, where the top boundary is simulated with the present-day sea level and the water table at the ground surface. The effect of the open tunnels on the head field at repository depth is an increased head around most of the repository tunnels (Figure 4-13). This is since the open tunnels, simulated by the specified-head internal boundary condition, transmit groundwater with high head from below the ice into the bedrock in front of the ice sheet. The exception is the north-western corner of the repository where the head in the surrounding bedrock is highest and where the open tunnels cause a smaller area of drawdown around the tunnel. The radius of influence (put in relation to the total head change) is of the same size as during the temperate conditions. The maximum head increase compared to the glacial reference closure case is about 200 m at the tunnels in south-east, where the distance from the ice front is largest.

4.2.2 Flow

Also in this case the effect of the open tunnels on flow at repository depth is visible as an increased flux in the nearest surrounding of the open tunnels and locally in deformation zones in contact with the tunnels (Figure 4-14 and Figure 4-15). The effect of larger spatial extent is also in this case seen in the southern repository area where there is an increased flux. No areas of decreased flux are observed at repository depth Figure 4-14 and Figure 4-15). An inspection of the vertical component of the flux (Figure 4-15 and Figure 4-16) shows that there is an increased upward flow in the deformation zones in contact with the open tunnels and in the southernmost deposition area due to the open tunnels. In the zone directly surrounding the tunnels, where water is injected from the open tunnels into the rock, there is mostly an increased downward flow. The explanation for this is that the studied horizontal plane is located slightly below the tunnels. The perspective view of the vertical flux field (Figure 4-16) also shows the general flow pattern with downward flow behind the ice front and upward flow ahead of the front with the transition between these some distance behind the front.

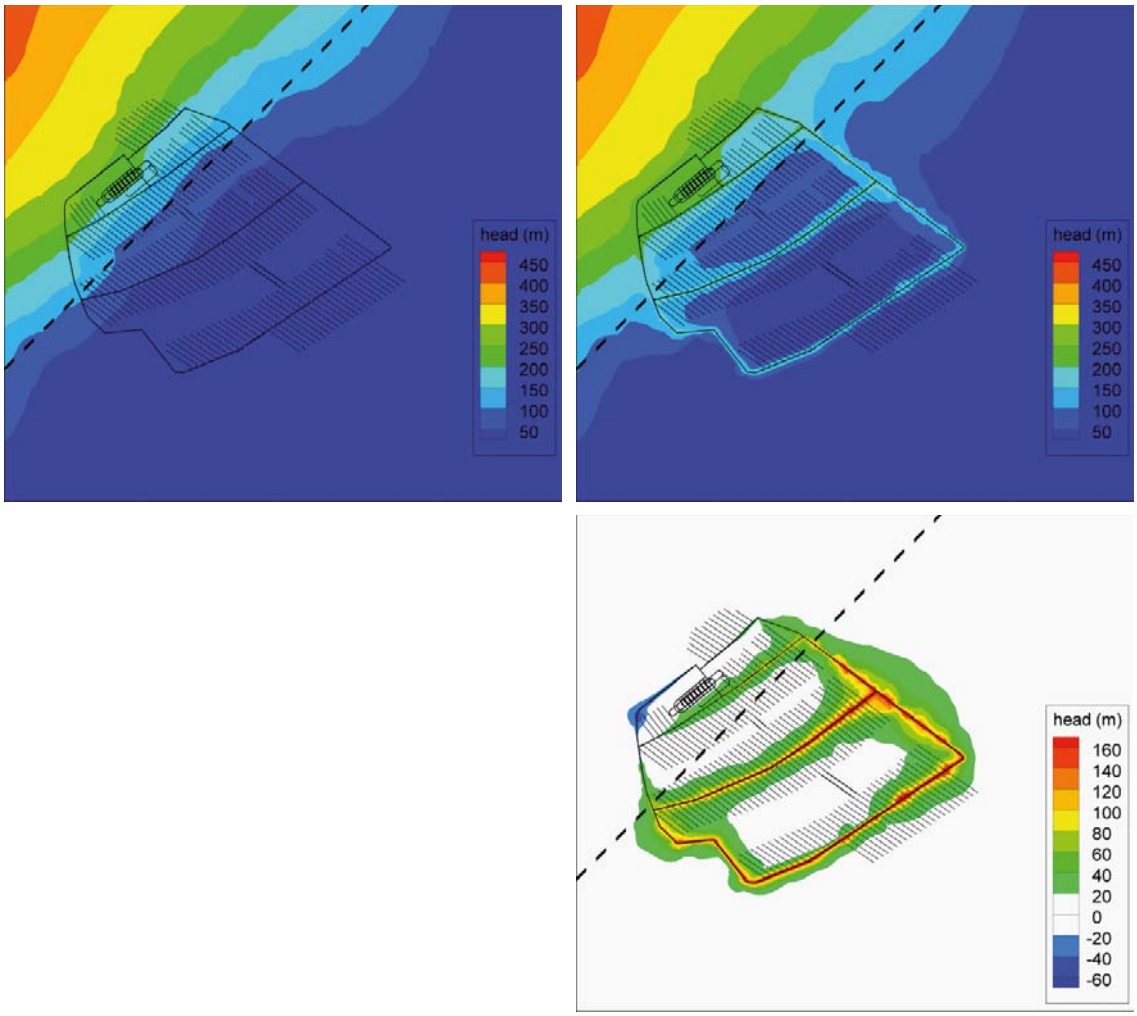

Figure 4-13. *Hydraulic head field at repository depth (Z = –465 m RHB 70) during glacial conditions for the reference closure case (upper left) and the open tunnel case (upper right). The datum level for head is 0 m RHB 70. The change in hydraulic head caused by the open tunnels is shown in the lower right image. The location of the ice front (IFL II) is shown by the dashed line.*

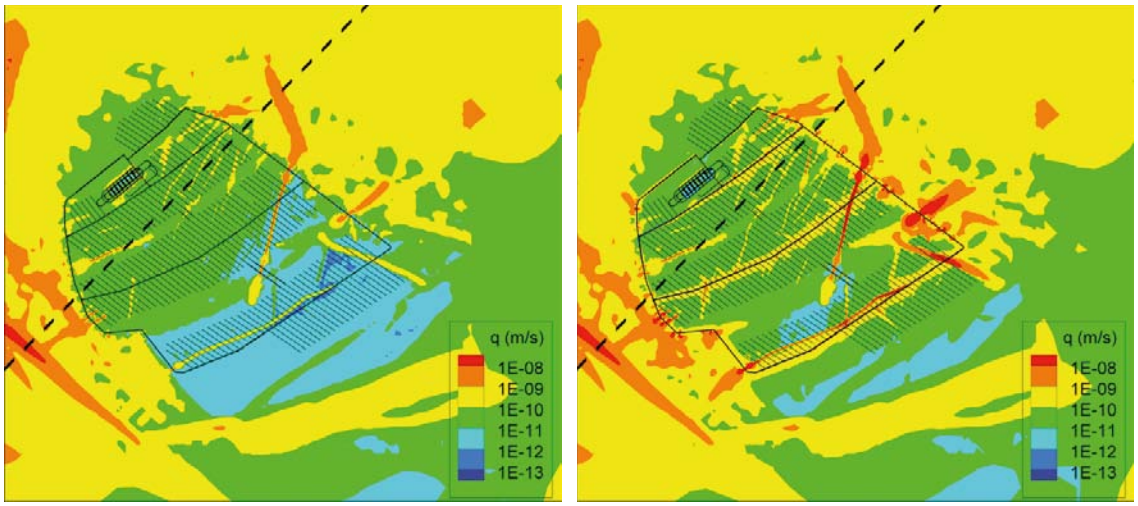

Figure 4-14. *Darcy flux magnitude at repository depth (Z = –465 m RHB 70) during glacial conditions for the reference closure case (left) and the open tunnel case (right). The location of the ice front (IFL II) is shown by the dashed line.*

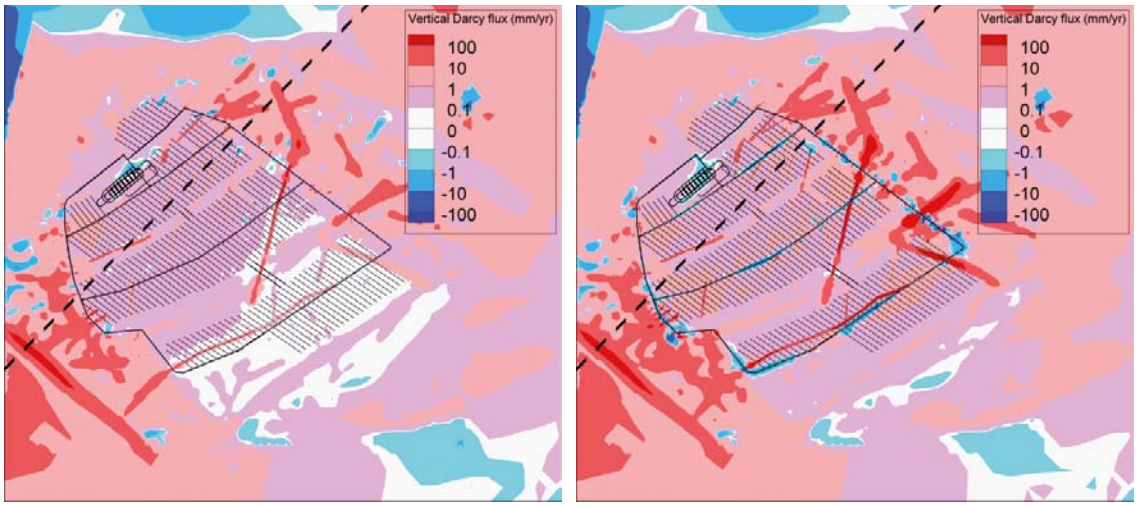

Figure 4-15. *Vertical Darcy flux in mm/yr at repository depth (Z = –465 m RHB 70) during glacial conditions for the reference closure case (left) and the open tunnel case (right). The location of the ice front (IFL II) is shown by the dashed line. Positive flux is directed upwards.*

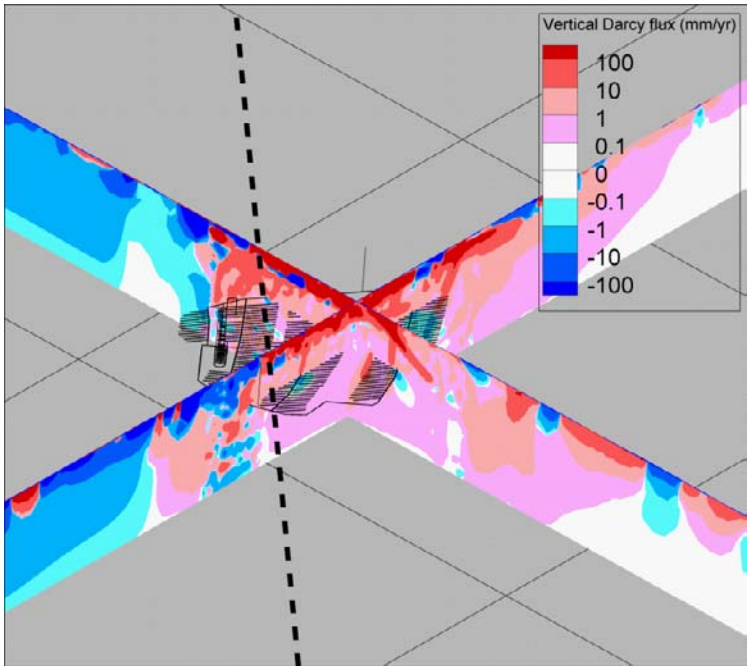

Figure 4-16. *Vertical Darcy flux in mm/yr during glacial conditions for the open tunnel case. View from south-west. The strike of the ice front (IFL II) is indicated by the dashed line. Positive flux is directed upwards.*

The distribution of flow between the open tunnels and the surrounding rock or soil is shown in Figure 4-17. The general pattern of flow through the tunnel system at repository level, as governed by the glacial top boundary condition, is inflow to the repository tunnel system through the ramp and shafts in the central area and discharge through the ventilation shafts in the deposition area, with some injection of water from the pressurized open tunnels into the surrounding bedrock. That is, there is a reversed direction of flow through the tunnel system compared to the temperate situation. The net rate of injection of water from the tunnels into the bedrock was calculated with the groundwater flow model to approximately 80 L/s. The flow through the open tunnel system during the glacial case is described in Chapter 3.2.2.

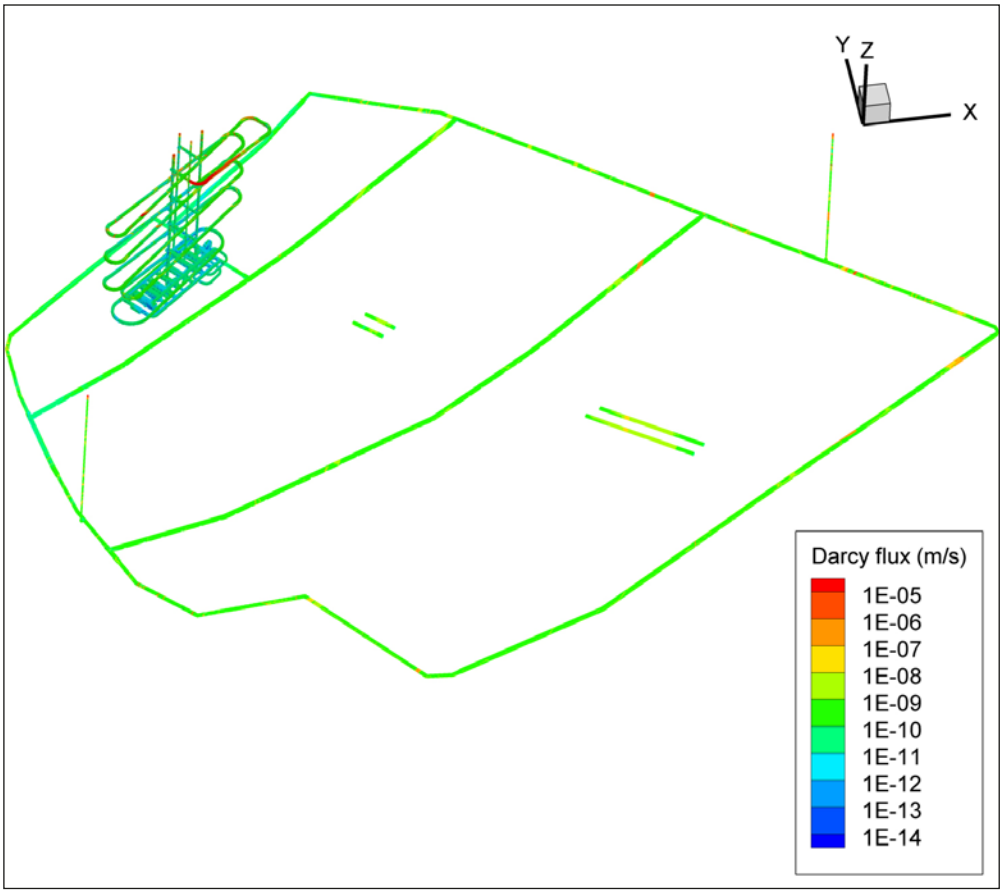

Figure 4-17. *Magnitude of Darcy flux between open tunnels and the surroundings during glacial conditions.*

A measure of the effect on the total turnover of groundwater in the rock volume containing the repository (below Z = –40 m) was that the sum of outflow over the outer boundary of the defined control volume surrounding the repository (see Section 4.1.2).The flow increased from 209 L/s to 223 L/s with the open tunnels, i.e. an increase of about 7%.

To conclude, in the temperate case the tunnels have lower head than the surrounding rock at depth, and the tunnels will acts as an easy path for groundwater from rock to surface. In the glacial case there is a higher head at surface that will be transmitted by the open tunnels to depth, and the tunnels will act as an injector of water into the bedrock.

4.2.3 Particle trajectories and discharge locations

The simulated discharge locations for the particles that reached the surface are shown in Figure 4-18 (tracking time 790,000 yr). In this figure, only particles that reached the surface through flow paths through the bedrock are shown. All discharge points are located south-east of the ice front. In contrast to the temperate case some discharge points are located on land. This is possible since in this case the land surface was a specified-head boundary which, due to the hydraulic gradient, allowed outflow. At the end of the tracking time 100% of the particles in the reference case and 99.7% of the particles in the open tunnel case had reached surface through flow paths in the bedrock. The full particle trajectories for 500 out of the 6,916 deposition hole positions are illustrated in Figure 4-19. The effects of open tunnels are not as apparent as for the temperate simulation, but open tunnels gave a larger spread of discharge points on land.

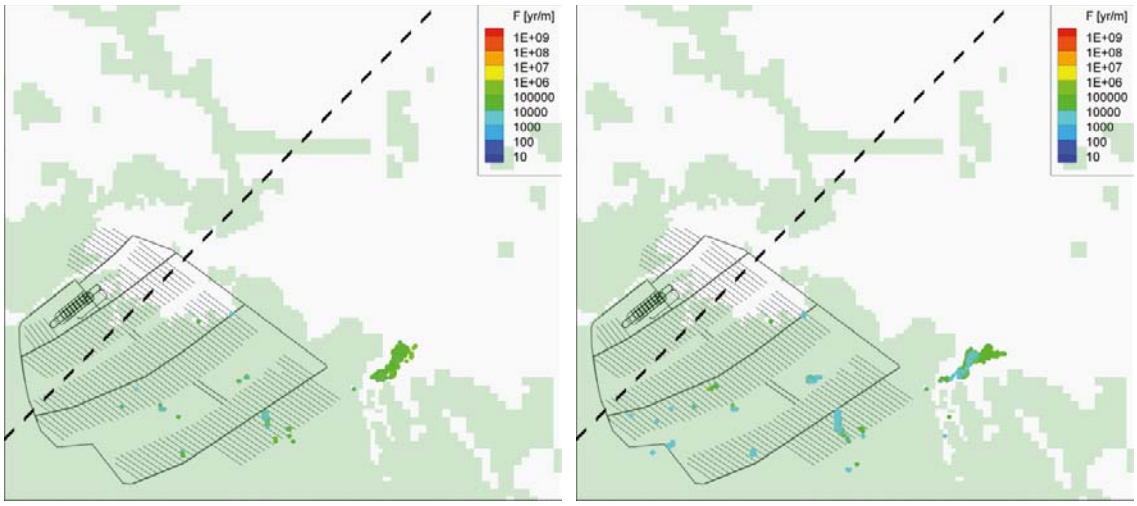

Figure 4-18. *Discharge locations at surface for particles released at the 6,916 deposition hole positions during glacial conditions for the reference closure case (left) and the open tunnel case (right). The exit points are coloured by the flow-related transport resistance (F-factor) for the flow path. The locations of the particles that entered open tunnels are not shown. The location of the ice front (IFL II) is shown by the dashed line.*

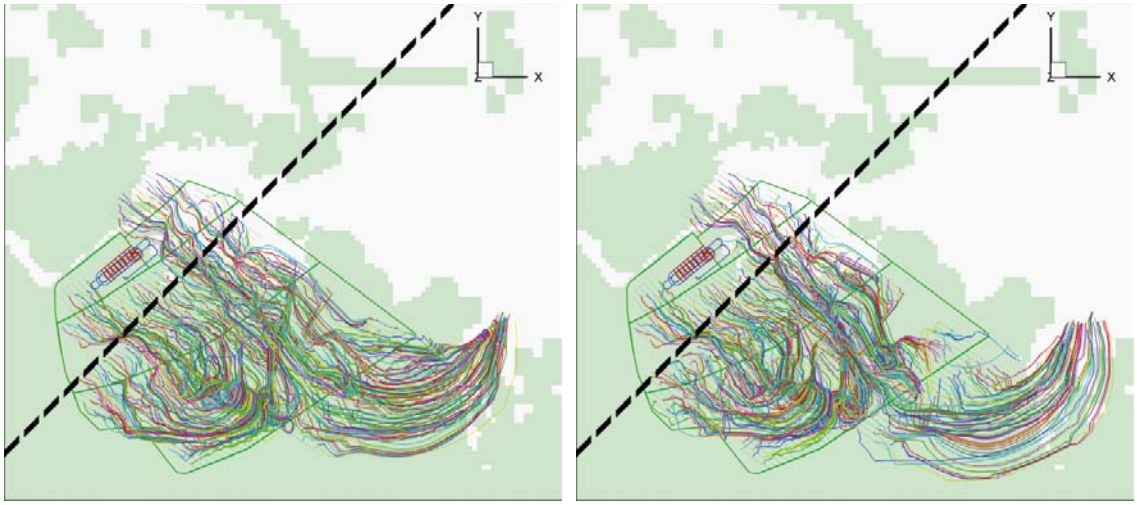

Figure 4-19. *Horizontal projection of trajectories for particles released at 500 of the 6,916 deposition hole positions during glacial conditions for the reference closure case (left) and the open tunnel case (right). The location of the ice front (IFL II) is shown by the dashed line.*

4.2.4 Discharge performance measures

The change in Darcy flux magnitude in the rock at the deposition holes due to open tunnels is significant (Figure 4-20). The median Darcy flux increased with about 100% from $5 \cdot 10^{-4}$ m/yr to $1 \cdot 10^{-3}$ m/yr, whereas the magnitudes of the lowest fluxes increased with a factor of 10. The latter is probably related to the earlier mentioned increased flux in the south-eastern deposition area seen in Figure 4-14.

All particles from the 6,916 deposition hole positions reached surface in the reference case and no entered the top sealing of the repository. In the open tunnel case, 99.7% of the particles reached surface. Of those only about 45 particles (0.7%) of the total number) entered open tunnels and thus reached surface through the tunnel system.

The flow-path lengths in the reference case are distributed between approximately 800 m and 4,400 m, with the median at about 1,900 m (Figure 4-21). Open tunnels caused some reduction in flow-path length; the median length is about 1,700 m. The shortest flow paths, below 500 m, represented the few particles that entered open tunnels. These particles entered the limited section of open tunnels in the northernmost part of the repository where the open tunnels gave a drawdown instead of an increased head.

The advective travel time to surface for the fastest particles was about 2 yr with the median at about 200 yr (Figure 4-22). The open tunnels gave some reduction in travel time, the median travel time decreased to about 30 yr, but the most apparent effect was that the distribution curve reshaped to a bi-modal form with one concentration of travel times at 10–30 yr and one concentration at about 1,000–5,000 yr.

The values of the flow-related transport resistance (F-factor) were above $1 \cdot 10^3$ yr/m in the reference case, with a median of $4 \cdot 10^4$ yr/m (Figure 4-23). The open tunnels decreased the median transport resistance with about 50% and also caused a few flow paths with a very low flow-related transport resistance, down to approximately 40 yr/m.

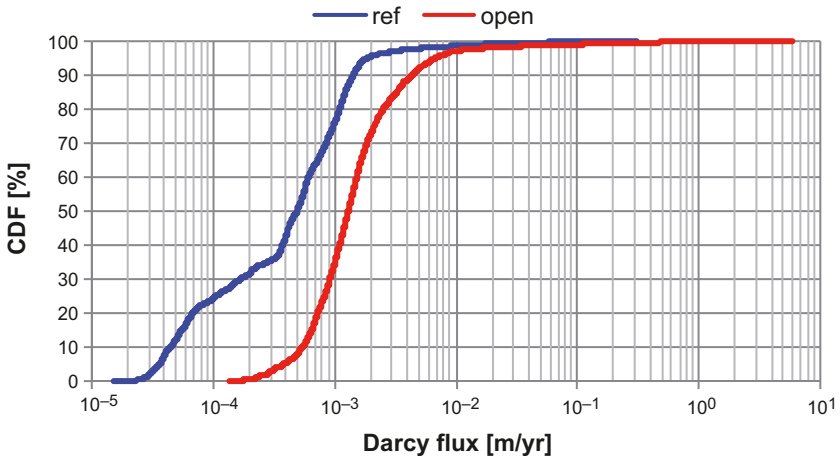

Figure 4-20. *Cumulative density function of simulated Darcy flux at the 6,916 deposition hole positions during glacial conditions for the reference closure case (blue) and the open tunnel case (red).*

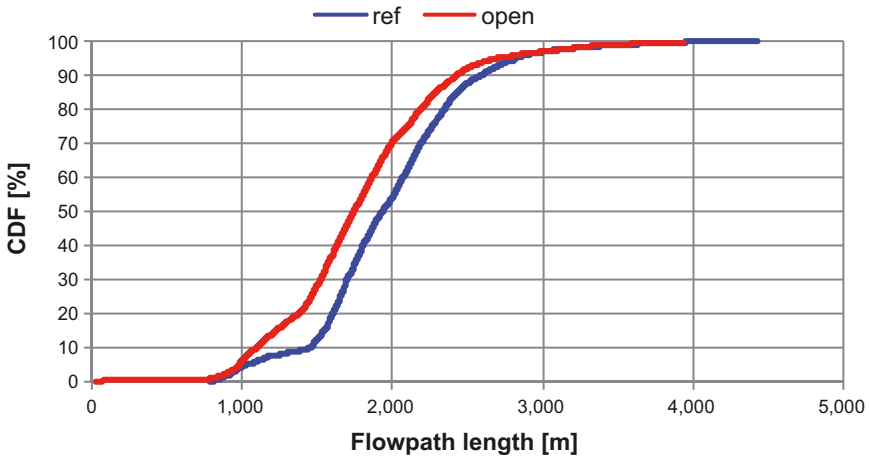

Figure 4-21. *Cumulative density function of simulated flow-path length for particles released at the 6,916 deposition hole positions during glacial conditions for the reference closure case (blue) and the open tunnel case (red).*

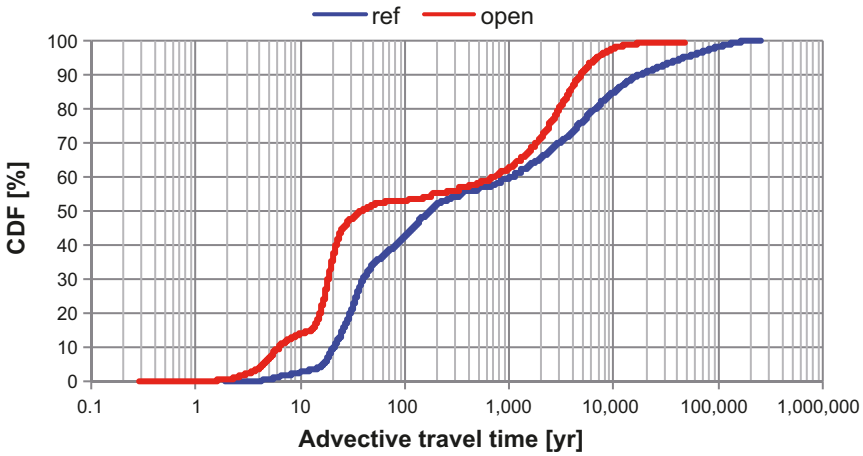

Figure 4-22. *Cumulative density function of simulated advective travel time for particles released at the 6,916 deposition hole positions during glacial conditions for the reference closure case (blue) and the open tunnel case (red).*

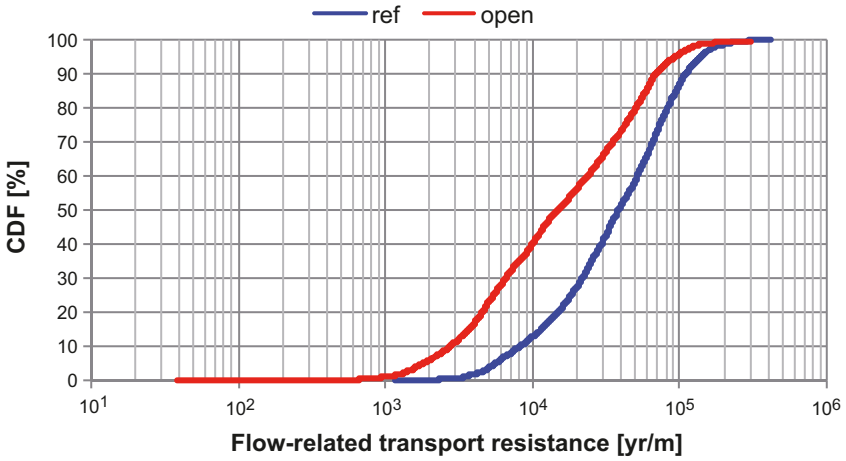

Figure 4-23. *Cumulative density function of simulated flow-related transport resistance (F-factor) for particles released at the 6,916 deposition hole positions during glacial conditions for the reference closure case (blue) and the open tunnel case (red).*

5 Discussion

5.1 Performance of the simulations

In order to assess the confidence in the simulation results presented above one may compare the results of the simulated reference closure cases to e.g. the results of the temperate simulations and of the glacial simulations for an advancing ice sheet without permafrost presented in /Vidstrand et al. 2010/:

- The simulated Darcy flux distribution at the deposition hole positions during temperate conditions (Figure 4-9) is in agreement with the distribution presented in /Vidstrand et al. 2010/.
- The pattern of vertical Darcy flux at repository depth (Figure 4-15) is very similar to the results by /Vidstrand et al. 2010/ for the glacial conditions. The agreement is not that good for the temperate conditions (Figure 4-3). The differences may be due to the different spatial resolution of the models and the different top boundary condition.
- The distributions of discharge locations at surface (Figure 4-7 and Figure 4-18) are very similar to the results by /Vidstrand et al. 2010/. The difference is that the model by /Vidstrand et al. 2010/ allows for some discharge also on land surface due to the different top boundary condition.
- The advective travel time of the particles for temperate conditions (Figure 4-11) are approximately 5 times longer in this study compared to the results by /Vidstrand et al. 2010/. This is expected since the minimum kinematic porosity applied in this study is 5 times larger than the porosity applied by /Vidstrand et al. 2010/. The other transport performance measures for the temperate conditions are difficult to compare since only about 40% of the particles were recovered at the end of tracking time at 1,000 yr in the simulation by /Vidstrand et al. 2010/.
- The range of flow-path lengths during glacial conditions in this study (Figure 4-21) is similar to those presented by /Vidstrand et al. 2010/. However, the shortest flow paths were less frequent in this study.
- There is a discrepancy between the advective travel time distributions for glacial conditions in this study (Figure 4-22) and in /Vidstrand et al. 2010/. The travel time is 20–30 times longer for shorter times and 200–300 times longer for longer times in this study compared to /Vidstrand et al. 2010/. A difference of a factor of 5 would have been expected (see above). Since the distributions of flow-path lengths and Darcy flux are similar, the hypothesis is that the apparent difference in advective travel time is due to either the differences in grid resolution between the models or to differences in the settings of the particle tracking algorithm.
- The distributions of the flow-related transport resistance (F-factor) are very similar (Figure 4-23 compared to the results in /Vidstrand et al. 2010/).

5.2 Hydraulic effects of open tunnels

It should be pointed out that the work presented here is a theoretical study that assesses a pessimistic scenario, i.e. these fully-open tunnel conditions are not expected to prevail in reality. The quantitative results should be considered to be of indicative character only, i.e. useful as a type of scoping calculation, especially for the rather hypothetical glacial scenario. There are a number of pessimistic assumptions in the analyses that are further discussed below.

In reality an initially open tunnel will collapse over time, and it seems very likely that rock and eroded material will fall down in the shafts and ramp and fill in at least parts of the open tunnels. Thus, the assumption of a completely open tunnel system is pessimistic. However, one can expect that the tunnel system will remain more permeable than the surrounding rock, and if there is a permeable tunnel system connected to surface, effects of open tunnels such as illustrated above may occur. Also, it is not the flow through the tunnels system (which is most sensitive to the permeability of the tunnels) that is most important for the performance of the repository that was studied here, but most important is the head difference between the open tunnels and the surrounding rock (which is

mostly governed by the driving head difference over the system). In the temperate case, the tunnels have lower head than the surrounding rock at depth, and the tunnels will acts as an easy path for groundwater from rock to surface. In the glacial case there is a higher head at surface that will be transmitted by the open tunnels to depth, and the tunnels will act as an injector of water into the bedrock.

One important uncertainty relates to the accessibility of water in the glacial case. In reality the flow in an open tunnel below the ice front will probably be limited by the supply of subglacial melt water in the transmissive subglacial layer /Vidstrand et al. 2010 and references therein/ at the ice-subsurface interface. If the supply of water is insufficient, there will be a drawdown of the pressure and the flow will decrease. The assumption of unlimited access of water below the ice is therefore pessimistic. In order to give such a high flow as illustrated above, the tunnel entrances have to coincide with a major melt water tunnel under the ice. Melt water tunnels are likely to form near the ice sheet margin though, and melt water from the ice surface may also reach the base of the ice through crevasses and moulins near the ice front /Vidstrand et al. 2010 and references therein/. However, an assessment of the probability to come across a melt water tunnel is outside the scope of this study.

Other possible effects of extreme water flow through an open repository tunnel system such as erosion of deposition tunnel plugs were not considered in this study. On the other hand, one may note that the situation with the ice front right above the repository is in reality a relatively short period. The speed of the advancing ice front may be 50 m/yr and the speed of the retreating ice front may be 100 m/yr /Vidstrand et al. 2010 and references therein/. The hydraulic gradient below the ice sheet when the repository is completely covered by ice may be even lower than during the temperate conditions /Vidstrand et al. 2010/.

6 Conclusions

The present study has shown that the hydraulic influence of abandoned open repository tunnels may be significant, considering the distribution of flow paths from the deposition holes studied. The performance measures of the different simulation cases are summarized in Table 6-1 and the quotient between the median results of the open tunnels cases to the reference closure cases are given in Table 6-2. However, it should be pointed out again that the study considers pessimistic cases and that the quantitative results should be considered to be of indicative character only.

Table 6-1. Summary of performance measures for discharged particles released at the 6,916 deposition hole positions for the studied simulation cases.

Case		Darcy flux at deposition positions [m/s]	Flow-path length [m]	Advective travel time [yr]	Flow-related transport resistance [yr/m]
Temperate – ref	(5^{th} perc)	$4.9 \cdot 10^{-14}$	650	392	$3.4 \cdot 10^{5}$
	(95^{th} perc)	$8.6 \cdot 10^{-13}$	2,387	>470,599	$2.4 \cdot 10^{7}$
	(median)	**$1.6 \cdot 10^{-13}$**	**1,297**	**2,744**	**$1.7 \cdot 10^{6}$**
Temperate – open		$5.0 \cdot 10^{-14}$	30	72	$2.0 \cdot 10^{4}$
		$1.2 \cdot 10^{-12}$	1,336	>788,387	$3.7 \cdot 10^{6}$
		$1.8 \cdot 10^{-13}$	**243**	**2,282**	**$5.0 \cdot 10^{5}$**
Glacial – ref		$1.2 \cdot 10^{-12}$	1,023	17	$5.6 \cdot 10^{3}$
		$5.9 \cdot 10^{-11}$	2,820	45,403	$1.4 \cdot 10^{5}$
		$1.6 \cdot 10^{-11}$	**1,928**	**172**	**$3.9 \cdot 10^{4}$**
Glacial – open		$1.2 \cdot 10^{-11}$	975	4	$1.8 \cdot 10^{3}$
		$2.1 \cdot 10^{-10}$	2,656	6,823	$8.9 \cdot 10^{4}$
		$4.1 \cdot 10^{-11}$	**1,737**	**37**	**$1.5 \cdot 10^{4}$**

Table 6-2. Quotients of the results for the open tunnels cases to the reference closure cases (median value open tunnels/median value reference closure).

Case	Darcy flux at deposition positions	Flow-path length	Advective travel time	Flow-related transport resistance
Temperate	1.13	0.19	0.83	0.29
Glacial	2.56	0.90	0.22	0.38

7 References

SKB's (Svensk Kärnbränslehantering AB) publications can be found at www.skb.se/publications.

Avis J, Clader N, Walsh R, 2009. Postclosure safety assessment (V1): Groundwater modelling. NWMO DGR-TR-2009-06, Nuclear Waste Management Organization, Canada.

Follin S, 2008. Bedrock hydrogeology Forsmark. Site descriptive modelling, SDM-Site Forsmark. SKB R-08-95, Svensk Kärnbränslehantering AB.

Harlow F H, Welsch J E, 1965. Numerical calculations of time-dependent viscous incompressible flow of fluid with free surface. Physics of Fluids, 8, 2182–2189.

Holmén J G, 1997. On the flow of groundwater in closed tunnels. Generic hydrogeological modelling of nuclear waste repository, SFL 3-5. SKB TR 97-10, Svensk Kärnbränslehantering AB.

Joyce S, Simpson T, Hartley L, Applegate D, Hoek J, Jackson P, Swan D, Marsic N, Follin S, 2010. Groundwater flow modelling of periods with temperate climate conditions – Forsmark. SKB R-09-20, Svensk Kärnbränslehantering AB.

Patankar S V, 1980. Numerical heat transfer and fluid flow. New York: Hemisphere. (Series in computational methods in mechanics and thermal sciences)

Rossman L A, 2000. EPANET 2 user's manual. EPA/600/R-00/057. U.S. Environmental Protection Agency, Washington, D.C.

Selroos J-O, Follin S, 2010. SR-Site groundwater flow modelling methodology, setup and results. SKB R-09-22, Svensk Kärnbränslehantering AB.

SKB, 2005a. Preliminary site description. Forsmark area – version 1.2. SKB R-05-18, Svensk Kärnbränslehantering AB.

SKB, 2005b. Forsmark site investigation. Programme for further investigations of geosphere and biosphere. SKB R-05-14, Svensk Kärnbränslehantering AB.

SKB, 2008. Site description of Forsmark at completion of the site investigation phase. SDM-Site Forsmark. SKB TR-08-05, Svensk Kärnbränslehantering AB.

SKB, 2010a. Design, production and initial state of the closure. SKB TR-10-17, Svensk Kärnbränslehantering AB.

SKB, 2010b. Handling of future human actions in the safety assessment SR-Site. SKB TR-10-53, Svensk Kärnbränslehantering AB.

Stephens M B, Fox A, La Pointe P R, Simeonov A, Isaksson H, Hermanson J, Öhman J, 2007. Geology Forsmark. Site descriptive modelling Forsmark stage 2.2. SKB R-07-45, Svensk Kärnbränslehantering AB.

Svensson U, Follin S, 2010. Groundwater flow modelling of the excavation and operational phases – Forsmark. SKB R-09-19, Svensk Kärnbränslehantering AB.

Svensson U, Ferry M, Kuylenstierna H-O, 2010. DarcyTools, Version 3.4. Concepts, methods and equations. SKB R-07-38, Svensk Kärnbränslehantering AB.

Vidstrand P, Follin S, Zugec N, 2010. Groundwater flow modelling of periods with periglacial and glacial climate conditions – Forsmark. SKB R-09-21, Svensk Kärnbränslehantering AB.

Appendix A

Compilation of input data to the DarcyTools groundwater flow model

Input data	Use[1)]	File name and version/property value	Source
Geometry CA and lower part of hoist and skip shafts	1	191BC_00_3001_FFM01.dat	Trac (CFE)
Geometry and upper part of hoist and skip shafts	1	191BC_00_3001_FFM02.dat	Trac (CFE)
Geometry lower part of ventilation shafts CA	1	191BC_00_3002_FFM01.dat	Trac (CFE)
Geometry upper part of ventilation shafts CA	1	191BC_00_3002_FFM01.dat	Trac (CFE)
Geometry lower part ramp	1	191BR_00_3001_FFM01.dat	Trac (CFE)
Geometry upper part ramp	1	191BR_00_3001_FFM02.dat	Trac (CFE)
Geometry lower part west ventilation shaft	1	191BSA00_4201_1_FFM01.dat	Trac (CFE)
Geometry upper part west ventilation shaft	1	191BSA00_4201_1_FFM02.dat	Trac (CFE)
Geometry lower part east ventilation shaft	1	191BSA00_4201_2_FFM01.dat	Trac (CFE)
Geometry upper part east ventilation shaft	1	191BSA00_4201_2_FFM02.dat	Trac (CFE)
Geometry model domain outside FFM	1	domffm.dat 2008-10-16	Trac (CFE)
Geometry FFM1 bot	1	FFM1bot.dat	Trac (CFE)
Geometry FFM1 mid	1	FFM1middle.dat	Trac (CFE)
Geometry FFM1 top	1	FFM1top.dat	Trac (CFE)
Geometry FFM2	1	FFM2.dat	Trac (CFE)
Geometry FFM3 bot	1	FFM3bot.dat	Trac (CFE)
Geometry FFM3 top	1	FFM3top.dat	Trac (CFE)
Geometry FFM4 bot	1	FFM4bot.dat	Trac (CFE)
Geometry FFM4 top	1	FFM4top.dat	Trac (CFE)
HCD (fracture file in format for deterministic fractures for DT)	1	HCD 2008-11-05	Trac (CFE)
Sheet joints (fracture file in format for deterministic fractures for DT)	1	HCDcage 2009-05-23	Trac (CFE)
Geometry watercourses	1	rivers.dat riversm2.dat riversp2.dat 2008-10-16	Trac (CFE)
Geometry deposition tunnels NW	1	Scenario1_DO_13.dat	Trac (CFE)
Geometry main and transport tunnels NW	1	Scenario1_ST.dat	Trac (CFE)
Geometry deposition tunnels central rep.	1	Scenario2_DO_13.dat	Trac (CFE)
Geometry main and transport tunnels central rep.	1	Scenario2_ST.dat	Trac (CFE)
Geometry deposition tunnels SE	1	Scenario3_DO_13.dat	Trac (CFE)
Geometry main and transport tunnels SE	1	Scenario3_ST.dat	Trac (CFE)
DFN set 1–15 (fracture file in format for deterministic fractures for DT)	1	set1to15.dat	Trac (CFE)
DFN set 16–24 (fracture file in format for deterministic fractures for DT)	1	set16to24.dat	Trac (CFE)
DFN set 25–34 (fracture file in format for deterministic fractures for DT)	1	set25to34.dat	Trac (CFE)
DFN set 35–50 (fracture file in format for deterministic fractures for DT)	1	set35to50.dat	Trac (CFE)
Topography	1	top.dat 2008-10-16	Trac (CFE)
Geometry water divide	1	WD.dat 2008-10-16	Trac (CFE)
Deposition hole positions	1	090220_fs_Q1_2000_fpc.csv	Trac (Serco)
Depth surface layer	1	20 m	Model delivery CFE 2010-01-15

Input data	Use[1)]	File name and version/property value	Source
Hydraulic conductivity in surface layer	1	$K_h = \max \begin{cases} 1\cdot10^{-7}\ \text{m/s} \\ 5\cdot10^{-3}\ \ 10^{-depth/3\ \text{m}}\ \ \text{m/s} \end{cases}$ $K_v = 1\cdot10^{-6}$ m/s	Model delivery CFE 2010-01-15
Hydraulic conductivity watercourses	1	$K_h = 2\cdot10^{-1}$ m/s	Model delivery CFE 2010-01-15
Hydraulic conductivity in rock, minimum	1	$1\cdot10^{-10}$ m/s	Model delivery CFE 2010-01-15
Hydraulic conductivity in rock outside FFM	1	depth< 200 m K = $1\cdot10^{-7}$ m/s 200 m < depth < 400 m K = $1\cdot10^{-8}$ m/s depth > 400 m K = $3\cdot10^{-9}$ m/s	Model delivery CFE 2010-01-15
Kinematic porosity in surface layer	1	$\theta = \max \begin{cases} 1\cdot10^{-3} \\ 5\cdot10^{-2}\ \ 10^{-depth/20\ \text{m}} \end{cases}$	Model delivery CFE 2010-01-15
Kinematic porosity in rock		$\theta = \max \begin{cases} 5\cdot10^{-5} \\ 5\cdot frevol/vol \end{cases}$	Model delivery CFE 2010-01-15
Kinematic porosity backfilled tunnels (deposition tunnels and other tunnels/shafts)	1	0.45	/Joyce et al. 2010/
Kinematic porosity central area	2	0.27	/Joyce et al. 2010/
Kinematic porosity open tunnels	3	1.0	Assumption
FWS in FFM	1	0.3 m^2/m^3 FFM01, FFM06 top 0.08 m^2/m^3 FFM01, FFM06 mid 0.02 m^2/m^3 FFM01, FFM06 bot 0.66 m^2/m^3 FFM02 0.18 m^2/m^3 FFM03, FFM05 top 0.10 m^2/m^3 FFM03, FFM05 bot 0.18 m^2/m^3 FFM04 top 0.10 m^2/m^3 FFM04 bot	/Vidstrand et al. 2010/
FWS backfilled tunnels	1	0 m^2/m^3	/Joyce et al. 2010/
FWS open tunnels	3	0 m^2/m^3	Assumption
Top boundary condition land	1	R = 130 mm/yr = $4.1\cdot10^{-9}$ m/s	Model delivery CFE 2010-01-15
Top boundary condition glacial case	4	• Water pressure at ground surface below ice sheet 92% of ice sheet thickness according to eq. 2-9 in R-09-21 • In front of ice sheet, above sea level: P = 0 at ground surface • In front of ice sheet, below sea level (z = 0): P hydrostatic	/Vidstrand et al. 2010/

1 = All cases
2 = Only reference cases
3 = Only open tunnel cases
4 = Only glacial cases

Trac (CFE) Path: SR-Site Data Storage/CFE/Forsmark/NiclasB20100309.zip
Trac (Serco) Path: SR-Site Data Storage/SERCO / Pathlines /090220_fs_Q1_2000_fpc.csv

Documentation of the EPANET 2 pipe network model for the Forsmark repository

The EPANET 2 pipe network model of the Forsmark repository is outlined in the figure below and documented in the tables on the following pages. The arrows on the link (tunnel) elements indicate the calculated direction of flow.

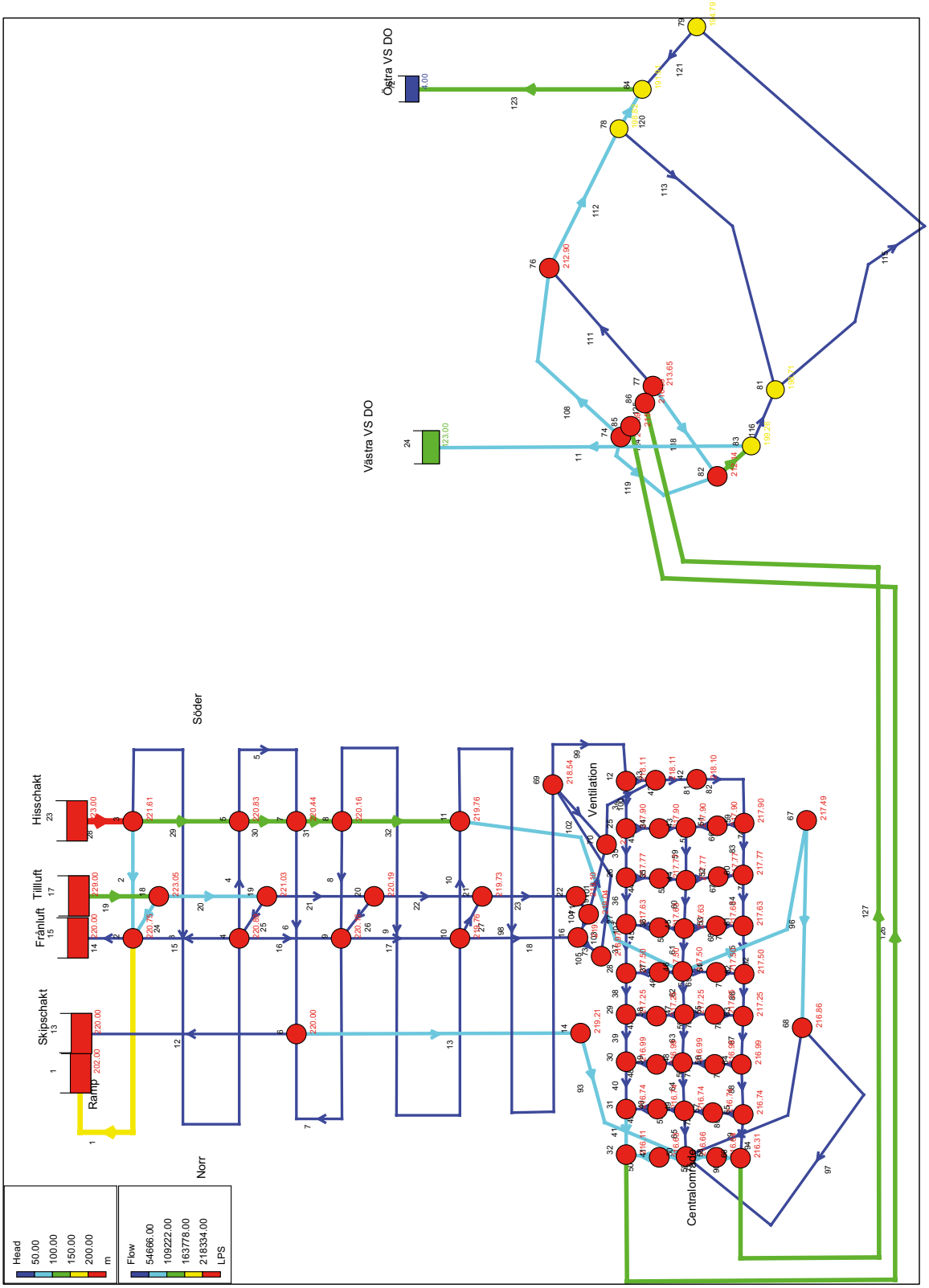

```
*************************************************************************
*                            E P A N E T                                *
*                      Hydraulic and Water Quality                      *
*                      Analysis for Pipe Networks                       *
*                            Version 2.0                                *
*************************************************************************
```

Input File: Forsmark_used.net

Link - Node Table:

Link ID	Start Node	End Node	Length m	Diameter mm
1	1	2	520	5600
2	2	3	70	5600
3	3	4	900	5600
4	4	5	70	5600
5	5	7	420	5600
6	7	6	150	5600
7	6	9	425	5600
8	9	8	70	5600
9	8	10	900	5600
10	10	11	70	5600
12	13	6	215	5000
13	6	14	220	5000
14	15	2	50	2500
15	2	4	100	2500
16	4	9	100	2500
17	9	10	100	2500
18	10	16	80	2500
19	17	18	50	3500
20	18	19	100	3500
21	19	20	100	3500
22	20	21	100	3500
23	21	22	80	3500
24	2	18	67	4400
25	4	19	67	4400
26	9	20	67	4400
27	10	21	67	4400
28	23	3	55	6000
29	3	5	100	6000
30	5	7	50	6000
31	7	8	50	6000
32	8	11	100	6000
34	12	25	30	5800
35	25	26	30	5800
36	26	27	30	5800
37	27	28	30	5800
38	28	29	30	5800
39	29	30	30	5800

Link - Node Table: (continued)

Link ID	Start Node	End Node	Length m	Diameter mm
40	30	31	30	5800
41	31	32	30	5800
42	12	33	30	5800
43	25	34	20	5800
44	26	35	20	5800
45	27	36	20	5800
46	28	37	20	5800
47	29	38	20	5800
48	30	39	20	5800
49	31	40	20	5800
50	32	41	20	5800
51	34	43	31	14900
52	35	44	27	14900
53	36	45	31	11700
54	37	46	31	9600
55	38	47	31	9500
56	39	48	31	9600
57	40	49	31	9600
58	41	50	31	8000
59	43	44	30	3400
60	44	45	30	3400
61	45	46	30	3400
62	46	47	30	3400
63	47	48	30	3400
64	48	49	30	3400
65	49	50	30	3400
66	43	51	31	14900
67	44	52	27	14900
68	45	53	31	11700
69	46	54	31	9600
70	47	55	31	9500
71	48	56	31	9600
72	49	57	31	9600
73	50	58	31	8000
74	51	59	20	5800
75	52	60	20	5800
76	53	61	20	5800
77	54	62	20	5800
78	55	63	20	5800
79	56	64	20	5800
80	57	65	20	5800
81	33	42	30	8400
82	42	59	40	5800
83	59	60	30	5800
84	60	61	30	5800
85	61	62	30	5800
86	62	63	30	5800

Link - Node Table: (continued)

Link ID	Start Node	End Node	Length m	Diameter mm
87	63	64	30	5800
88	64	65	30	5800
89	65	66	30	5800
90	66	58	20	5800
91	11	46	100	6000
92	46	67	20	6000
93	14	50	25	5000
94	50	68	26	5000
96	68	67	145	5800
97	50	68	105	5800
98	11	69	1075	5600
99	69	12	175	5600
100	33	70	40	4100
101	70	71	135	4400
102	69	70	40	4400
103	16	71	10	4400
104	71	22	10	4400
105	16	73	20	4400
107	73	69	145	4400
108	74	76	1890	7500
111	76	77	1502	7500
112	76	78	1358	5800
113	78	81	3783	7500
115	79	81	5694	7500
116	81	83	237	5800
117	83	82	723	5800
118	82	77	1444	7500
119	82	74	1629	7500
120	78	84	666	5800
121	84	79	975	5800
123	84	72	466	3000
124	74	85	70	5800
125	77	86	60	5800
126	32	85	20	5800
127	66	86	20	5800
11	83	24	463	3000

Node Results:

Node ID	Demand LPS	Head m	Pressure m	Quality
2	0.00	220.75	278.75	0.00
3	0.00	221.61	283.61	0.00
4	0.00	220.89	220.89	0.00
5	0.00	220.83	220.83	0.00
6	0.00	220.00	220.00	0.00
7	0.00	220.44	220.44	0.00
8	0.00	220.16	220.16	0.00
9	0.00	220.16	220.16	0.00
10	0.00	219.76	219.76	0.00
11	0.00	219.76	219.76	0.00
12	0.00	218.11	218.11	0.00
14	0.00	219.21	219.21	0.00
16	0.00	219.03	219.03	0.00
18	0.00	223.05	281.05	0.00
19	0.00	221.03	221.03	0.00
20	0.00	220.19	220.19	0.00
21	0.00	219.73	219.73	0.00
22	0.00	219.10	219.10	0.00
25	0.00	217.90	217.90	0.00
26	0.00	217.77	217.77	0.00
27	0.00	217.63	217.63	0.00
28	0.00	217.50	217.50	0.00
29	0.00	217.25	217.25	0.00
30	0.00	216.99	216.99	0.00
31	0.00	216.74	216.74	0.00
32	0.00	216.11	216.11	0.00
33	0.00	218.11	218.11	0.00
34	0.00	217.90	217.90	0.00
35	0.00	217.77	217.77	0.00
36	0.00	217.63	217.63	0.00
37	0.00	217.50	217.50	0.00
38	0.00	217.25	217.25	0.00
39	0.00	216.99	216.99	0.00
40	0.00	216.74	216.74	0.00
41	0.00	216.63	216.63	0.00
42	0.00	218.10	218.10	0.00
43	0.00	217.90	217.90	0.00
44	0.00	217.77	217.77	0.00
45	0.00	217.63	217.63	0.00
46	0.00	217.50	217.50	0.00
47	0.00	217.25	217.25	0.00
48	0.00	216.99	216.99	0.00
49	0.00	216.74	216.74	0.00
50	0.00	216.66	216.66	0.00
51	0.00	217.90	217.90	0.00
52	0.00	217.77	217.77	0.00
53	0.00	217.63	217.63	0.00

Node Results: (continued)

Node ID	Demand LPS	Head m	Pressure m	Quality	
54	0.00	217.50	217.50	0.00	
55	0.00	217.25	217.25	0.00	
56	0.00	216.99	216.99	0.00	
57	0.00	216.74	216.74	0.00	
58	0.00	216.64	216.64	0.00	
59	0.00	217.90	217.90	0.00	
60	0.00	217.77	217.77	0.00	
61	0.00	217.63	217.63	0.00	
62	0.00	217.50	217.50	0.00	
63	0.00	217.25	217.25	0.00	
64	0.00	216.99	216.99	0.00	
65	0.00	216.74	216.74	0.00	
66	0.00	216.31	216.31	0.00	
67	0.00	217.49	217.49	0.00	
68	0.00	216.86	216.86	0.00	
69	0.00	218.54	218.54	0.00	
70	0.00	218.52	218.52	0.00	
71	0.00	219.04	219.04	0.00	
73	0.00	218.97	218.97	0.00	
74	0.00	214.59	214.59	0.00	
76	0.00	212.90	212.90	0.00	
77	0.00	213.65	213.65	0.00	
78	0.00	198.82	198.82	0.00	
79	0.00	194.79	194.79	0.00	
81	0.00	198.71	198.71	0.00	
82	0.00	212.14	212.14	0.00	
83	0.00	199.26	199.26	0.00	
84	0.00	191.91	191.91	0.00	
85	0.00	215.77	215.77	0.00	
86	0.00	216.09	216.09	0.00	
1	180230.00	202.00	0.00	0.00	Reservoir
13	1401.34	220.00	0.00	0.00	Reservoir
15	22188.58	220.00	0.00	0.00	Reservoir
17	-154022.00	229.00	0.00	0.00	Reservoir
23	-295514.60	223.00	0.00	0.00	Reservoir
72	150032.60	4.00	0.00	0.00	Reservoir
24	95684.03	123.00	0.00	0.00	Reservoir

Link Results:

Link ID	Flow LPS	Velocity m/s	Unit Headloss m/km	Status
1	-180230.00	7.32	36.06	Open
2	-105075.80	4.27	12.27	Open
3	26782.75	1.09	0.80	Open
4	27459.60	1.11	0.84	Open
5	28635.81	1.16	0.92	Open
6	51479.27	2.09	2.95	Open
7	-18127.90	0.74	0.37	Open
8	-3206.07	0.13	0.01	Open
9	19842.38	0.81	0.44	Open
10	4270.03	0.17	0.02	Open
12	-1401.34	0.07	0.00	Open
13	68205.84	3.47	3.60	Open
14	-22188.58	4.52	15.01	Open
15	-6547.76	1.33	1.37	Open
16	15402.87	3.14	7.30	Open
17	11296.27	2.30	3.97	Open
18	17237.84	3.51	9.12	Open
19	154022.00	16.01	118.92	Open
20	63226.85	6.57	20.23	Open
21	40599.36	4.22	8.41	Open
22	29784.13	3.10	4.56	Open
23	39414.90	4.10	7.93	Open
24	-90795.11	5.97	34.38	Open
25	-22627.49	1.49	2.15	Open
26	-10815.24	0.71	0.49	Open
27	9630.78	0.63	0.39	Open
28	295514.60	10.45	25.28	Open
29	163656.10	5.79	7.81	Open
30	162479.90	5.75	7.70	Open
31	139636.50	4.94	5.70	Open
32	116588.00	4.12	3.99	Open
34	45531.90	1.72	6.95	Open
35	36346.19	1.38	4.43	Open
36	36264.89	1.37	4.41	Open
37	36361.34	1.38	4.43	Open
38	50115.67	1.90	8.42	Open
39	50185.04	1.90	8.44	Open
40	50302.21	1.90	8.48	Open
41	60150.46	2.28	20.93	Open
42	1812.29	0.07	0.00	Open
43	9185.71	0.35	0.08	Open
44	81.29	0.00	0.00	Open
45	-96.44	0.00	0.00	Open
46	-13754.34	0.52	0.18	Open
47	-69.36	0.00	0.00	Open
48	-117.18	0.00	0.00	Open
49	-9848.25	0.37	0.09	Open

Link Results: (continued)

Link ID	Flow LPS	VelocityUnit m/s	Headloss m/km	Status
50	-75492.38	2.86	26.03	Open
51	9185.71	0.05	0.00	Open
52	81.29	0.00	0.00	Open
53	-96.44	0.00	0.00	Open
54	-13754.34	0.19	0.01	Open
55	-69.36	0.00	0.00	Open
56	-117.18	0.00	0.00	Open
57	-9848.25	0.14	0.01	Open
58	-75492.38	1.50	0.91	Open
59	15872.52	1.75	4.38	Open
60	15933.27	1.75	4.41	Open
61	15740.28	1.73	4.30	Open
62	22200.43	2.45	8.55	Open
63	22061.89	2.43	8.44	Open
64	22026.08	2.43	8.42	Open
65	12461.76	1.37	2.70	Open
66	-6686.81	0.04	0.00	Open
67	20.54	0.00	0.00	Open
68	96.55	0.00	0.00	Open
69	13754.34	0.19	0.01	Open
70	69.18	0.00	0.00	Open
71	-81.38	0.00	0.00	Open
72	-283.93	0.00	0.00	Open
73	60254.21	1.20	0.58	Open
74	-6686.81	0.25	0.04	Open
75	20.54	0.00	0.00	Open
76	96.55	0.00	0.00	Open
77	13754.34	0.52	0.18	Open
78	69.18	0.00	0.00	Open
79	-81.38	0.00	0.00	Open
80	-283.93	0.01	0.00	Open
81	42931.05	0.77	0.23	Open
82	42931.05	1.62	5.06	Open
83	36244.24	1.37	4.41	Open
84	36264.78	1.37	4.41	Open
85	36361.34	1.38	4.43	Open
86	50115.67	1.90	8.42	Open
87	50184.86	1.90	8.44	Open
88	50103.48	1.90	8.42	Open
89	49819.55	1.89	14.36	Open
90	-60254.21	2.28	16.58	Open
91	89047.83	3.15	22.55	Open
92	55078.99	1.95	0.91	Open
93	68205.84	3.47	101.94	Open
94	-26437.01	1.35	7.66	Open
96	-55078.99	2.08	4.32	Open
97	-28641.98	1.08	1.90	Open

Link Results: (continued)

Link ID	Flow LPS	Velocity m/s	Unit Headloss m/km	Status
98	31810.21	1.29	1.13	Open
99	47344.19	1.92	2.50	Open
100	-41118.75	3.11	10.42	Open
101	-30092.95	1.98	3.79	Open
102	11025.81	0.73	0.51	Open
103	-9321.95	0.61	0.37	Open
104	-39414.90	2.59	6.49	Open
105	26559.79	1.75	2.95	Open
107	26559.79	1.75	2.95	Open
108	59341.47	1.34	0.90	Open
111	-46973.80	1.06	0.50	Open
112	106315.30	4.02	10.37	Open
113	10783.19	0.24	0.03	Open
115	-54500.49	1.23	0.69	Open
116	-43717.30	1.65	2.35	Open
117	-139401.30	5.28	17.81	Open
118	-63099.98	1.43	1.05	Open
119	-76301.36	1.73	1.50	Open
120	95532.09	3.62	10.37	Open
121	-54500.49	2.06	2.95	Open
123	150032.60	21.23	403.24	Open
124	-135642.80	5.13	16.87	Open
125	-110073.80	4.17	40.58	Open
126	135642.80	5.13	16.87	Open
127	110073.80	4.17	11.11	Open
11	95684.03	13.54	164.71	Open